Lipid-mediated GPR32 signaling reprograms macrophage metabolism to impair anti-tuberculous immunity

Joaquina Barros[1,2,3], Mariano Maio[1,2,3], Martín Manuel Ledesma[2], María Emilia Boix[1], Natacha Faivre[3,4], Sarah Monard[3,4], José Luis Marín Franco[2], Arnaud Métais[4], Florencia Sabbione[2], Federico Fuentes[2], Tomas Martín Grosso[1], Agustina Juliana Errea[5], Xavier Aragone[6], Milagro Sanchez Cunto[6], Domingo Palmero[6], Mario Matteo[6], Matías Ostrowski[1], Rafael J Argüello[7], Ranjan Kumar Nanda[8], Emilie Layre[3,4], Olivier Neyrolles[3,4], Christel Vérollet[3,4], Geanncarlo Lugo Villarino[3,4†], and Luciana Balboa[1,2,3,*†]

[1] Instituto de Investigaciones Biomédicas en Retrovirus y SIDA (INBIRS). Facultad de Medicina. Universidad de Buenos Aires- Consejo Nacional de Investigaciones Científicas y Técnicas (CONICET), Buenos Aires, Argentina

[2] Instituto de Medicina Experimental (IMEX)-CONICET, Academia Nacional de Medicina, Buenos Aires, Argentina

[3] International Associated Laboratory (LIA) CNRS IM-TB/HIV (1167), Buenos Aires, Argentina / International Research Project Toulouse, France

[4] Institut de Pharmacologie et de Biologie Structurale (IPBS), Université de Toulouse, CNRS, UPS, Toulouse, France

[5] Instituto de Estudios Inmunológicos y Fisiopatológicos - CONICET - Universidad Nacional de La Plata, La Plata, Argentina

[6] Instituto Prof. Dr. Raúl Vaccarezza; Hospital de Infecciosas Dr. F.J. Muñiz, Buenos Aires, Argentina

[7] Aix-Marseille University, CNRS, INSERM, CIML, Centre d'Immunologie de Marseille-Luminy, Turing Centre for Living Systems, Marseille, France

[8] Translational Health Group, International Center of Genetic Engineering and Biotechnology, New Delhi, India

Corresponding Author: Luciana Balboa, Paraguay 2155, Piso 11 CABA (C1121ABG), Argentina, + 54(011) 4508-3689, luciana_balboa@hotmail.com

The authors have declared that no conflict of interest exists.

[†] These authors contributed equally to this work

Abstract

Mycobacterium tuberculosis, the causative agent of tuberculosis (TB), has evolved strategies to evade innate immunity and establish persistent infection. However, the mechanisms by which M. tuberculosis reprograms human macrophage metabolism remain incompletely defined. Tuberculous pleural effusion (TB-PE), a common extrapulmonary manifestation that frequently coexists with pulmonary TB, offers a unique, clinically relevant immunometabolic window into the TB microenvironment. Here, using patient-derived TB-PE samples, we demonstrate that this microenvironment induces a metabolic state in human macrophages that compromises their antimicrobial function. Lipidomic analysis identified an enrichment of the specialized pro-resolving mediator Resolvin D5 (RvD5), which signals through GPR32 to suppress macrophage microbicidal activity. The acellular fraction of TPE was sufficient to induce RvD5 secretion by monocytes, correlating with increased expression of RvD5 biosynthetic enzymes in pleural monocytes from TB patients. Mechanistically, RvD5-GPR32 signaling inhibited glycolysis without promoting oxidative phosphorylation, reducing HIF-1α activity and impairing intracellular M. tuberculosis control. HIF-1α stabilization restored antimicrobial function. These findings uncover the RvD5-GPR32-HIF-1α axis as a mechanism of metabolic immune suppression and a potential target for host-directed TB therapy.

Significance statement

Tuberculosis (TB) persists as a global threat because Mycobacterium tuberculosis hijacks host lipid metabolism to subvert immunity. This study investigates how TB-induced host lipids reprogram macrophage metabolism to weaken their antimicrobial activity. We show that tuberculous pleural effusion, a fluid accumulation in the pleural cavity, is enriched with the lipid mediator Resolvin D5 (RvD5). RvD5 impairs macrophage function by blocking glycolysis via the GPR32 receptor, leading to an energy-deficient state that compromises bacteria killing. Remarkably, restoring the metabolic regulator HIF-1α rescues this antimicrobial defect. By revealing a mechanism through which TB exploits host-derived lipids to evade immune control, this work deepens our understanding of infection-induced immune dysfunction and highlights potential

68 *therapeutic targets for TB and other infectious diseases.*

Introduction

The success of *M. tuberculosis* (Mtb) as a pathogen lies, in part, in its efficient adaptation to the intracellular environment of human macrophages, which involves the regulation of the host's metabolic pathways leading to immune evasion. Macrophages are essential immune cells that can serve as a niche for the intracellular persistence of mycobacteria, but at the same time possess the ability to limit infection by activating their microbicidal properties. In fact, innate immunity seems to be sufficient to clear Mtb infections in certain patients, conferring resistance[1]. This activation of macrophages towards the microbicidal program (called the M1 activation program) depends on a profound metabolic change that promotes glycolysis to the detriment of mitochondrial oxidative phosphorylation[2,3].

Tuberculous pleural effusion (TB-PE) is characterized by an accumulation of fluid in the pleural cavity of infected patients, marked by elevated levels of proteins, lipids, and specific leukocyte populations. Recent studies have begun to characterize the metabolites present in these samples, revealing a differential abundance of amino acids, citric acid cycle intermediates, and free fatty acids when compared to malignant pleural effusions[4]. TB-PE is typically a serous fluid and contains very few viable mycobacteria, indicating a paucibacillary infection. The development of TB-PE is likely caused by a low-burden mycobacterial infection in the pleural space, which typically originates from initial parenchymal lesions. This infection triggers an immune response that not only increases the production of pleural fluid but also impairs its drainage[5].

TB-PE is the second most prevalent form of extrapulmonary TB, after TB lymphadenitis, accounting for 15-25% of TB cases worldwide. In immunocompromised populations, it may represent as much as 50% of all cases[6]. Compared to samples obtained from blood or bronchoalveolar lavage (BAL) of TB patients, TB-PE provides a more accurate reflection of the microenvironment encountered during infection. It captures the specific cellular composition and environmental factors at the site of infection, which is anatomically related to the lungs. In fact, there is a significant association between pleural TB and pulmonary TB as coexisting parenchymal disease has been identified in 48%[7] and 86%[8] of computed tomography scans conducted on patients with pleural TB. Furthermore, TB-PE samples better represent the

physiological concentrations of metabolites and compounds since they are not diluted with saline, as is the case with BAL. These distinctive characteristics make TB-PE a valuable tool for research on TB.

While it has been suggested that -type-1 immunity is dominantly present in TB-PE[9], infection control within the pleural cavity is considered insufficient as patients frequently experience recurrent episodes of TB if left untreated[10]. This raises the possibility of active mechanisms that impede the development of a long-term protective immune response. In this regard, we demonstrated that the acellular fraction of TB-PE induces the differentiation of monocytes into immunosuppressive macrophages[11–13], converting them into lipid-laden or foamy macrophages, thus affecting their effector functions against bacilli[14]. We have also demonstrated that microbicidal M1 macrophages exposed to a lipid fraction isolated from TB-PE, enriched in metabolites derived from polyunsaturated fatty acids (PUFA), are unable to carry out the metabolic reprogramming associated with their pro-inflammatory profile, showing reduced glycolytic activity, as well as increased mitochondrial respiration and reduced microbicidal activity[15]; however, the mechanism of action as well as the specific metabolites involved in this effect remain unclear, limiting the potential to develop targeted therapies aimed at enhancing anti-TB immune response.

As an exudate in response to infection, both inflammatory and pro-resolving processes are deployed in TB-PE. Among the mechanisms aimed at limiting the inflammatory process and activating tissue repair and healing are those catalyzed by a family of lipids recently termed "specialized resolution lipid mediators" or SPMs[16]. SPMs derive from PUFA such as linoleic acid (C18: Δ2, n-6), arachidonic acid (C20: Δ4, n-6), eicosapentaenoic acid (EPA, 20:5, n-3) and docosahexaenoic acid (DHA, 22:6, n-3), which are produced through enzymatic reactions catalyzed by lipoxygenases (LOX) and/or cyclooxygenases (COX). SPMs are composed of DHA-derived D-series protectins and resolvins, EPA-derived E-series resolvins and arachidonic acid-derived lipoxins.

By binding to specific receptors, resolvins modulate various inflammatory processes, including neutrophil migration, macrophage phagocytosis, and the expression of pro-inflammatory mediators, thereby mitigating inflammatory pathologies[17]. The G protein-coupled receptor 32 (GPR32) has been shown to bind to resolvins RvD1, RvD3, and RvD5[18–20]. Although direct evidence

supporting the RvD5-GPR32 axis in lung infections remains limited, investigations into related resolvins, such as RvD1[21], yield promising results in models of lung injury, indicating reduced neutrophil infiltration and diminished alveolar damage. These findings strongly implicate the RvD1-GPR32 axis as a critical regulatory pathway. This mechanism is especially pertinent in the context of bacterial pneumonia and viral infections, like influenza, where a carefully calibrated immune response is essential. Despite the known importance of resolvins, to date, there is no study investigating the role of RvD5 in TB. In this study, we performed a lipidomic analysis of TB-PE and found high levels of the lipid mediator RvD5. We characterize its function by exposing M1 macrophages to this lipid mediator and found that RvD5 is sufficient to impair their microbicidal activity and their glycolytic metabolism in M1 macrophages. We functionally validate that this impairment is mediated by the direct binding between RvD5 and its receptor GPR32, expressed in macrophages, whose activation inhibits HIF1α. Restoring HIF1α with a chemical activator was sufficient to rescue the functionality of M1 macrophages exposed to RvD5.

Material and methods

Human Subjects

Buffy coats from healthy donors were prepared at Centro Regional de Hemoterapia Garrahan (Buenos Aires, Argentina) according to the institutional guidelines (resolution number CEIANM-664/07). Informed consent was obtained from each donor before blood collection.

Pleural effusions (PE) were obtained by therapeutic thoracentesis by physicians at the Hospital F. J Muñiz (Buenos Aires, Argentina). The diagnosis of TB pleurisy was based on a positive Ziehl–Neelsen stain or Löwenstein–Jensen culture from PE and/or histopathology of pleural biopsy, and was further confirmed by an Mtb-induced IFNγ response and an adenosine deaminase-positive test[10]. None of the patients had multidrug-resistant TB. For this study, we used acellular fractions of PE stored at -80°C for lipid determination, and fresh paired pleural fluids and blood mononuclear cells (PFMC and PBMC) for the assessment of the metabolic profiles and GPR32 expression. PE samples were divided according to their etiology. We prepared pools of the acellular fraction from 10 to 12 patients with tuberculous PE labeled as “TB-PE pool 1 and 2,” respectively; six patients with malignant PE (PE-C) including mesothelioma, lung carcinoma or metastatic PE; eight patients with parapneumonic PE (PE-PNI); and five patients with transudates secondary to heart failure (HF-PE).

The research was carried out in accordance with the Declaration of Helsinki (2013) of the World Medical Association and was approved by the Ethics Committee of the Hospital F. J Muñiz (protocol number: NIN-2520-23). Written informed consent was obtained before sample collection.

Bacterial strain

The Mtb laboratory strain, H37Rv, was grown at 37°C in Middlebrook 7H9 medium supplemented with 10% albumin-dextrose-catalase (both from Becton Dickinson, New Jersey, USA) and 0.05% Tween-80 (Sigma-Aldrich, St. Louis, MO, USA). The red fluorescent protein (RFP)-expressing Mtb strain was gently provided by Dr. Fabiana Bigi (INTA, Castelar, Argentina).

Preparation of PE pools

The PE were collected in heparin tubes and pools of the acellular fractions were prepared, as previously described[15].

Preparation of human monocyte-derived Macrophages

Monocytes were isolated from PBMC, as previously described[15], and differentiated in the presence of human recombinant Granulocyte-Macrophage Colony-Stimulating Factor (GM-CSF, Peprotech, New York, USA) at 50 ng/ml. Cells were allowed to differentiate for five to seven days into M0 macrophages.

Macrophages treatments

Macrophages were polarized toward M1 profile with IFNγ (10 ng/ml) plus LPS (10 ng/ml), exposed (or not) to either RvD5 (33 nM), vehicle (ethanol), or 20% v/v of PE during 24 h to generate M1 and treated-M1 cells, respectively. When indicated, macrophages were pre-incubated with GPR32 blocking antibodies (10 µg/mL; GTX71225, GeneTex), or their rabbit IgG isotype control (GeneTex) for 30 minutes prior to exposure with RvD5. Alternatively, M1 macrophages were generated only with IFNγ and either stimulated with Mtb γ-irradiated H37Rv strain (NR-49098, BEI Resources, USA) (equivalent to a multiplicity of infection “MOI” of 1:1) or infected with Mtb, and exposed (or not) to RvD5 (33 nM) for 24 h. Also, when specified, cells were exposed (or not) to DMOG (200 µM) during LPS or Mtb infection for 24 h.

Determination of lactate

Lactate production in the culture medium was measured using the Lactate Kit from Wiener (Argentina). The absorbance was read using a Biochrom Asys UVM 340 Microplate Reader microplate reader and software.

Lipids preparation and lipidomic analysis of PUFAs from TB-PE

Lipids extractions from TB-PE were based on Bligh and Dyer protocol, as previously described[15].

PUFA were then extracted on solid phase as follow. 40 µL of internal standards mixture (Deuterium labeled compounds) were added to the lipid extracts resuspended in 260 uL of cold methanol. After centrifugation at 5000 g for 15

minutes at 4°C, supernatants were transferred into 2 mL 96-well deep plates and diluted in H_2O to 2 mL. Samples were submitted to solid phase extraction (SPE) using OASIS HLB 96-well plate (30 mg/well, Waters) pretreated with MeOH (1mL) and equilibrated with 10% MeOH (1 mL). After sample application, extraction plate was washed with 10% MeOH (1 mL). After drying under aspiration, lipids mediators were eluted with 1 mL of MeOH. Prior to LC-MS/MS analysis, samples were evaporated under nitrogen gas and reconstituted in 20 µL on MeOH.

The samples were analyzed at the MetaToul lipidomic platform (I2MC, INSERM 1048, Toulouse, France) on a LCMS8060 (Shimadzu) using a Kinetex C18 column (1.7µm, 1 x 100 mm; Phenomenex). The mobile phases consisted of 0.1% formic acid (FA) in H_2O as mobile phase A and 0.1% FA in acetonitrile (ACN) as mobile phase B. Data were acquired in Multiple Reaction Monitoring (MRM) mode with optimized conditions (ion optics and collision energy). Peak detection, integration and quantitative analysis were done using Insight software (Shimadzu) based on calibration lines built with commercially available standards (Cayman Chemicals).

<u>Determination of intracellular SPMs</u>

Monocytes from buffy coats of healthy donors were stimulated with TB-PE 20% v/v for 30 minutes and then cell extracts were performed to monitor RvD5 abundances. Cells were washed with ice-cold PBS (without Mg^{2+} and Ca^{2+}) and scraped in ice-cold methanol/5 mM EGTA (2:1 v/v) snap-frozen in liquid nitrogen and then stored at -80°C until SPE and LC-MS analysis, performed as described above.

<u>SCENITH assays</u>

SCENITH experiments were performed using the SCENITH kit containing all reagents and anti-puromycin antibodies (www.scenith.com). Briefly, PFMCs, PBMCs, and macrophages were treated for 40 minutes at 37°C in the presence of the indicated inhibitors of various metabolic pathways and puromycin. After the incubation, puromycin was stained using fluorescently labeled anti-Puromycin monoclonal antibodies (clone R4743L-E8) with either Alexa Fluor

647 or Alexa Fluor 488, and analyzed by flow cytometry. The impact of the various metabolic inhibitors was quantitated, as previously described[22,23].

Measurement of cell respiration with Seahorse flux analyzer

Bioenergetics in human macrophages were determined using a Seahorse XFe24 analyzer. ATP production rates and relative contribution from glycolysis and oxidative phosphorylation (OXPHOS) were measured by the Seahorse XF Real-Time ATP Rate Assay kit. Macrophages (250,000 cells/well) were cultured in triplicates per condition. The assay was performed in XF Assay Modified DMEM. Three consecutive measurements were performed under basal conditions and after the sequential addition of oligomycin (OM) and rotenone together with antimycin (ROT/AA) (Agilent, USA). Extracellular acidification (ECAR) and oxygen consumption rates (OCR) were measured. Mitochondrial ATP production rate was determined by the decrease in the OCR after oligomycin addition. Conversely, the complete inhibition of mitochondrial respiration with rotenone plus antimycin A allows accounting for mitochondrial-associated acidification, and when combined with proton efflux rate (PER) data, it allows calculation of Glycolysis ATP production rate. All OCR and ECAR values were normalized. Briefly, before the assay, brightfield imaging was performed. Cellular area per condition was calculated by ImageJ software and imported into Wave (Agilent) using the normalization function.

Additionally, Mito Stress Test was performed to measure the rate of mitochondrial oxidative phosphorylation. Basal respiration was calculated as the last measurement before addition of OM minus the non-mitochondrial respiration, which is the minimum rate measurement after addition of ROT/AA. Estimated ATP production designates the last measurement before addition of OM minus the minimum rate after OM. Maximal respiration rate (Max) was defined as the OCR after addition of OM and FCCP at 2µM (for 2.5 minutes). Spare respiratory capacity (SRC) was defined as the difference between max and basal respiration. Three consecutive measurements were performed under basal conditions and after the sequential addition of the following electron transport chain inhibitors.

RNA-Single Cell sequencing analysis

Previously published single cell transcriptomic data available in Genome Sequence Archive in the BIG Data Center, Beijing Institute of Genomics, Chinese Academy of Sciences, under accession numbers HRA000910 and HRA00036[24], was used to evaluate the expression of enzymes involved in SMPs' biosynthesis (ALOX5, ALOX12, ALOX 15 and ALOX15B), including five paired samples from PBMC and PFMC from TB patients. The Seurat package version 4.3.0.1 of the RStudio software was used to read the pre-processed files. The filtering process involved discarding cells with fewer than 200 or more than 5000 total genes, as well as cells with fewer than 200 or more than 20,000 total counts, and those with mitochondrial read levels above 10%. Expression levels were then normalized using the log (scale.factor = 10,000), considering the 2,000 most variable genes. The samples were integrated using the reciprocal PCA (RPCA) algorithm. The different cell clusters were identified using the shared nearest neighbor (SNN) modularity optimization algorithm, and dimensionality reduction was performed using the UMAP (Uniform Manifold Approximation and Projection) algorithm. Individual cells were annotated using the SingleR package version 2.2.0 and the HumanPrimaryCellAtlasData database (label.fine version).

Intracellular expression of HIF1α

Macrophages were permeabilized with triton 0.3% in FACS buffer and incubated with PE-anti-HIF1α (clone 546-16, Biolegend) for 30 minutes. After that, cells were analyzed by flow cytometry using the FACSCalibur cytometer (BD Biosciences, San Jose, CA, USA). The macrophage population was gated according to its Forward and Size Scatter properties. The median fluorescence intensity (MFI) was analyzed using FCS Express V3 software (*De Novo* Software, Los Angeles, CA, USA).

GPR32 surface expression

To monitor GPR32 expression in $CD14^+$ cells from pleural effusion and blood paired samples of TB vs. non-TB patients, cells were incubated with a primary anti-GPR32 antibody (GTX71225; GeneTex) for 40 minutes at 4°C. Next, the cells were incubated with a secondary antibody to label anti-GPR32 (Alexa Fluor 488; anti-Rabbit IgG; 111-546-144). After an anti-CD14-PerCP/Cy7 (clone

HCD14, Biolegend) was employed and the cell viability marker zombie violet (Biolegend).

Fluorescence microscopy

Fluorescence microscopy images of fixed IFNγ-activated (M1) macrophages exposed (or not) to RvD5 that were first infected with Mtb-RFP (MOI 1-3:1) for 24 h and then fixed. Cell nuclei were labeled with DAPI, and the autophagy marker LC3 protein (anti-LCE3B; dilution 1:300; #NB100-2220) was identified by indirect immunofluorescence using Alexa Fluor 488 conjugated antibodies, whereas the late endosome marker, LAMP2, was identified by indirect immunofluorescence using an specific conjugated antibody (anti-LAMP2 Alexa Fluor 633; dilution 1:200; #A21126). Samples were imaged on a FluoView FV1000 confocal microscope (Olympus, Tokyo, Japan) equipped with a Plapon 60X/NA1.42 objective and on the Zeiss LSM 800 confocal microscope (Zeiss, Oberkochen, Germany).

IL-1β determination

The amount of human IL-1β was measured by ELISA, according to the manufacturer's instructions kits (ELISA MAX Deluxe Kits from Biolegend). The detection limit was 15.6 pg/ml.

Infection of human macrophages with Mtb

Infections were performed in the biosafety level 3 laboratories at the *Unidad Operativa Centro de Contención Biológica (UOCCB), ANLIS-MALBRAN* (in 2022) and at *Instituto de Investigaciones Biomédicas en Retrovirus y SIDA (INBIRS)-CONICET-UBA* (in 2023-24), according to the biosafety institutional guidelines (both institutes located in Buenos Aires). Macrophages were infected with Mtb H37Rv strain at a MOI of 0.5-3:1 during 1 h at 37°C. Next, extracellular bacteria were removed gently by washing with pre-warmed PBS, and cells were cultured in RPMI-1640 medium supplemented with 10% FBS and gentamicin (50 µg/ml). The extracellular bacteria were then removed gently by washing with pre-warmed PBS, and cells were cultured in RPMI-1640 medium supplemented with 10% FBS and gentamicin (50 µg/ml) for 4, 24 and 72h. At different time points, macrophages were lysed in 0.1% SDS and neutralized with 20% BSA in

Middlebrook 7H9 broth. Serial dilutions of the lysates were plated in triplicate, onto 7H11-Oleic Albumin Dextrose Catalase (OADC, Becton Dickinson) agar medium for CFU scoring at 21 days later.

Immunohistochemistry of nonhuman primate lung samples

All animal procedures were approved by the Institutional Animal Care and Use Committee of Tulane University, New Orleans, LA and were performed at the Tulane TNPRC, and under approval from IACUC (project numbers P3733, P3794, P3373 and P3628). They were performed in strict accordance with NIH guidelines. The two adult rhesus macaques used in this study were bred and housed at the Tulane National Primate Research Center (TNPRC), and infections were described in[13,25]. For histological stainings, paraffin embedded lung samples were sectioned (4µm, Leica RM 2035) and, after rehydration successively in histo-clear II (National diagnostics), ethanol (100;90;70;50%), water, the sections were unmasked in 10mM citrate pH6 20 minutes at 106-110°C for heat antigen retrieval. After saturated in goat serum 5% - BSA 5%, triton X100 0.2% (GTX73249 Genetex, 4-100-812-C Euromedex, T8787sigma) 1 h at room temperature, the sections were stained with primary antibodies anti-GPR32 (GTX71225; GenteTex, 1:50) and anti-CD68 Alexa Fluor 647 ([KP1], sc-20060 A647 Santacruz, 1:50) at 4°C overnight. After several washing in PBS, the sections were stained with secondary antibody anti-rabbit Alexa Fluor 555 (cell signaling #4413S, 1:400) for 2 h at room temperature, and after washing, the nuclei are stained with DAPI (Sigma D9542) for 5 minutes. The slides were mounted with a fluorescent mounting medium (S3023 DAKO). Images were acquired using a Axio Imager M2 (Zeiss) microscope, ORCA-flash 4.0 LT (Hamamatsu) camera, X20/0.8 Plan Apochromat objective (Zeiss) and processed using Zen software (Zeiss).

Quantification and Statistical Analysis

Data are presented as scatter plots with each circle representing an individual. Means are displayed with standard error of the mean (SEM). Each independent experiment corresponds to one donor. Comparisons between paired experimental conditions were conducted using the two-tailed Wilcoxon Signed-Rank Test for non-parametric data, or a t-test for parametric data. A two-way

ANOVA, followed by Dunnett's multiple comparisons test, was employed to compare two or more experimental groups against a single control group. Alternatively, a two-way ANOVA followed by Holm-Sidak's multiple comparisons test was utilized to compare multiple conditions in the presence (or not) of blocking antibodies against GPR32. To compare all conditions with one another, a two-way ANOVA followed by Tukey’s multiple comparisons test, or a two-way ANOVA followed by the two-stage linear step-up procedure of Benjamini, Krieger, and Yekutieli, was performed to control for multiple comparisons. Additionally, the Mann-Whitney U test was used to compare the metabolic profiles of pleural $CD14^+$ cells from unpaired TB patients undergoing treatment to those not receiving treatment. Fisher's exact test was performed to analyze the levels of RvD5 produced by TB-PE-treated monocytes, since in untreated cells the levels were consistently below the detection limit. Correlation analyses were conducted using Spearman’s rank correlation coefficient. A p-value of less than 0.05 was considered statistically significant.

Results

Enrichment in specialized resolution lipid mediators correlates with impaired macrophage glycolysis in tuberculous pleural effusions.

We previously found that PUFA metabolites in TB-PE inhibit the glycolytic activity of M1 macrophages[15]. To explore whether this inhibition was specific to pleural TB lipids, we compared the ability of the PUFA extracted from the acellular fraction of TB-PE and non-TB patients to inhibit glycolysis in M1 macrophages (activated by IFNγ and LPS), by assessing lactate release from these cells. The lipid fractions isolated from TB-PE showed enhanced inhibition of lactate release by M1 macrophages compared to PE from non-tuberculous patients affected by other pathologies such as heart failure, pneumonia, and cancer (**Figure 1A**). To further investigate the candidate components responsible for this inhibition, a targeted lipidomic analysis was conducted on lipids isolated from TB and non-TB patients (n=13 and 5, respectively). Among the 36 screened PUFA metabolites, four exhibited significantly higher levels in TB-PE compared to non-TB PE (**Figure 1B-C**). Notably, these molecules were specialized resolution lipid mediators (SPMs) derived from omega-3 fatty acids, i.e., 7 Maresin R1 (7MaR1), RvD5, Protectin Dx (PDx), and 18-HEPE (**Figure 1B-C**). Furthermore, the abundance of these SPMs significantly correlated with the decline in glycolysis induced by each PE when tested on monocyte-derived M1 macrophages from healthy donors (**Figure 1D**). Our data indicate that SPMs are highly present in TB-PE and their levels correlate with TB-PE capacity to suppress M1 macrophage glycolytic activity.

Monocytes synthesize RvD5 and macrophages express GPR32 in Tuberculous Contexts

Our next objective was to investigate the potential origins of SMPs in the TB-PE. To address this, we analyzed the expression of key enzymes involved in SPM biosynthesis, namely arachidonic acid 5-lipoxygenase (5-LO, ALOX5) along with arachidonic acid 12- and 15-lipoxygenating paralogues (ALOX12, ALOX15, and ALOX15B)[26], in peripheral blood mononuclear cells (PBMC) and pleural fluid mononuclear cells (PFMC) from TB patients. This analysis utilized publicly available single-cell RNA-Seq datasets (accession numbers HRA000910 and HRA00036). According to the literature[27], lymphocytes

(especially T cells) dominate leukocyte infiltrates, while monocytic populations are underrepresented in TB-PE compared to blood (**Figure 2A)**. Although no significant levels of ALOX12, ALOX15 and ALOX15B transcripts were detected in monocytes from both compartments, our findings revealed an upregulation of ALOX5 in $CD14^+$ pleural cells (monocytes and monocyte-derived cells) compared to circulating $CD14^+$ monocytes (**Figure 2B-C and Figure S1-2**). This suggests that $CD14^+$ pleural cells are the predominant mononuclear cell population contributing to the local resolvin production in the pleural cavity.

We also examined RvD5 levels in monocytes obtained from healthy donors exposed to the acellular fraction of TB-PE and compared to unexposed monocytes. RvD5 was significantly detected in extracts from monocytes treated with the acellular fraction of TB-PE (**Figure 2D**). Together, these findings indicate that monocytes produce RvD5 in response to environmental factors present in the pleural cavity of pleural TB patients.

Building on these results, we next explore the potential involvement of the RvD5-GPR32 axis in pleural TB pathogenesis. Previous studies have shown that GPR32 is highly expressed on macrophages and its activation induces macrophage polarization from a pro-inflammatory to a pro-resolutive phenotype[28]. In line with these findings, we confirmed the physiological relevance of GPR32 expression by measuring higher expression levels of GPR32 in $CD14^+$ cells isolated from the pleural cavity compared to circulating $CD14^+$ cells (**Figure 2E-F**). This demonstrates the receptor's expression in cells locally exposed to RvD5.

To expand to other TB-impacted tissues, we analyzed the expression of GPR32 in lung samples from non-human primates with TB granulomas[13,25]. Within granuloma where $CD68^+$ macrophages accumulate and form the classical multinucleated giant cells, we detected GPR32 expression in a subset of $CD68^+$ macrophages (**Figure 2G**). These results suggest that the key components of the RvD5-GPR32 axis are present in macrophages within tuberculous contexts.

The RvD5-GPR32 axis mediates the inhibition of macrophage glycolysis by tuberculous pleural effusions

To determine whether RvD5 was responsible for the inhibition of macrophage glycolysis triggered by TB-PE, we conducted functional assays using commercially available RvD5. As previously shown[29], compared to non-activated macrophages (M0), M1 macrophages typically exhibited high glycolytic activity by increasing lactate release (**Figure 3A**). When physiological doses of RvD5 (17 and 33nM), usually found in TB-PE, were added to M1 macrophages, it efficiently inhibited lactate production similarly to TB-PE (**Figure 3A and S3A**). Notably, RvD5 treatment did not affect cell viability (**Figure S3B**). Given the pivotal role of HIF1α in the TB-PE-induced impairment of M1 macrophage functions[15], we explored whether RvD5 influenced the upregulation of HIF1α in M1 cells. Our findings revealed that RvD5 reduced HIF1α expression in M1 macrophages (**Figure 3B**). Similarly, RvD5 suppressed lactate release when M1 macrophages (activated by IFNγ) were challenged with irradiated *M. tuberculosis* (**Figure 3C**).

Given the high expression of GPR32 observed in $CD14^+$ pleural cells, we investigated whether the inhibitory effects of exogenous RvD5 are mediated through this receptor. First, in line with the literature[30], we confirmed the expression of GPR32 in M1 macrophages (**Figure 3D**). Next, we observed that blocking GPR32 fully restored lactate release in M1 macrophages exposed to either RvD5 or TB-PE (**Figure 3E**), indicating that GPR32 signaling by TB-PE lipids was sufficient to alter the metabolism of M1 macrophages. Moreover, blockade of GPR32 also restored HIF1α levels in both RvD5 and PE-treated M1 macrophages (**Figure 3F)**.

These findings collectively demonstrate that RvD5 inhibits glycolysis in M1 macrophages through a GPR32-dependent mechanism, suppressing HIF1α activity.

Activation of the RvD5-GPR32 axis reduces glycolysis without affecting mitochondrial bioenergetics in M1 macrophages

To investigate if the TB-associated microenvironment affects the metabolic profile of pleural monocyte/macrophages, we compared the *ex vivo* metabolic profile of $CD14^+$ cells from TB-PE with those from pleural effusions of other etiologies (nonTB-PE). This was achieved by monitoring changes in protein translation upon treatment with oligomycin and/or 2-deoxy-D-glucose using the SCENITH assay[23]. Our findings indicated a reduced glycolytic capacity in cells residing in the TB pleural cavity compared to blood cells (**Figure 4A and Figure S4A**). Interestingly, pleural macrophages from TB patients undergoing antibiotic treatment exhibited a significant increase in glycolysis compared to those untreated patients (**Figure 4A**). Consistent with our previous findings showing that TB patients display elevated glycolysis in their systemic monocytes[22], this study further highlights a significant increase in glycolytic activity in the blood of patients with pleural TB (**Figure 4A**). Notably, this heightened glycolysis tends to normalize with antibiotic treatment, resembling the glycolytic profile of circulating monocytes in patients with non-TB pleural effusions (**Figure 4A**).

Additionally, we evaluated the impact of RvD5 on the relative contributions of metabolic pathways to the cellular energy metabolism of M1 macrophages using SCENITH. According to the expected glycolytic profile of M1 activation program[31], M1 macrophages exhibited a lower reliance on OXPHOS alongside an increase in the glycolytic capacity compared to unstimulated cells (M0) (**Figure 4B**). However, this metabolic shift in M1 macrophages was impaired upon addition of exogenous RvD5 **(Figure 4B and Figure S4B-C)**. Of note, while TB-PE has been shown to promote lipid body accumulation in macrophages[11,14], RvD5 did not induce lipid body formation, at least at the tested doses **(Figure S5**). These findings indicate that RvD5 reduces the glycolytic activity of M1 macrophages independently of lipid body accumulation, unlike TB-PE.

To examine the effect of RvD5 on the OXPHOS metabolic state in macrophages, we performed the Seahorse XF Cell Mito Stress Test in M0, M1 and RvD5-treated M1 cells. To characterize the overall energy phenotypes of these macrophages, basal oxygen consumption rate (OCR) was plotted against extracellular acidification rate (ECAR). The resulting metabolic phenogram

revealed that RvD5 shifts the energy metabolism of M1 macrophages towards a less glycolytic profile without impacting aerobic metabolism (**Figure S6A**). This shift is further reinforced by the significant decrease in basal ECAR levels observed in RvD5-treated M1 cells compared to untreated M1 cells (**Figure 4C**), aligning with the metabolic characterization from SCENITH and lactate measurements described earlier (**Figure 3A and 4B**).

Analysis of respiratory parameters indicate substantial reductions in ATP-linked OCR and maximal respiratory capacity in M1 macrophages compared to M0 cells, alongside slight decreases in basal respiration and spare respiratory capacity and a marginal increase in non-mitochondrial respiration. However, these respiratory parameters were unaffected by RvD5 treatment, except for a further reduction in maximal respiratory capacity induced by the lipid (**Figure 4D**).

To further evaluate intracellular ATP production, we measured the basal ECAR and OCR to calculate ATP production rates from glycolysis (GlycoATP) and mitochondrial OXPHOS (MitoATP). M1 macrophages exhibited higher ATP production rates from glycolysis compared to RvD5-treated M1 macrophages (**Figure S6A, C-D**), with no differences in ATP production from mitochondrial respiration (**Figure S6A-B and D**). Consistent with SCENITH findings, the relative contribution of MitoATP to total ATP production increased, while the contribution of GlycoATP decreased in RvD5-treated M1 macrophages compared to untreated M1 cells (**Figure 4E**). Furthermore, in line with these results, while M1 macrophages showed lower mitochondrial mass compared to control cells, this parameter remained unchanged upon RvD5 treatment **(Figure S7A-B)**. Similarly, transmission electron microscopy (TEM) revealed no differences in mitochondrial morphology between RvD5-treated and untreated M1 macrophages (**Figure S7C**). These findings suggest that RvD5 reduces glycolysis without increasing aerobic metabolism, thereby promoting a less energetically active metabolic state.

Finally, we assessed whether specific inhibition of GPR32 could restore M1 metabolism in RvD5-treated macrophages. Our results revealed that blocking

GPR32 caused a notable shift in RvD5-M1 cells, driving them towards heightened glycolysis, as evidenced by an increase in basal ECAR (**Figure 4F and Figure S8A and C**). Notably, key respiratory parameters, including basal OCR and maximal respiratory capacity, were significantly diminished in RvD5-M1 macrophages following GPR32 inhibition (**Figure 4G**), suggesting a compensatory reduction in OXPHOS to accommodate the increased glycolysis. These findings were further corroborated by ATP production analysis, which yielded a significant increase in GlycoATP levels and a corresponding decrease in MitoATP levels upon GPR32 inhibition (**Figure S8B-D**). Additionally, the relative contribution of GlycoATP to total ATP production was enhanced, while the contribution of MitoATP decreased, compared to cells treated with the isotype control (**Figure 4H**). This metabolic reprogramming highlights a pronounced shift towards glycolytic reliance at the expense of the OXPHOS activity.

Collectively, these results underscore the critical role of the RvD5-GPR32 axis in suppressing the glycolytic activity of M1 macrophages, maintaining a hypometabolic state without enhancing OXPHOS flux.

RvD5 boosts a pro-resolving phenotype in M1 macrophages at the expense of its mycobacterial control potential

Since RvD5 is a SPMs, we assessed the acquisition of pro-resolutive features by M1 macrophages exposed to RvD5. M1 macrophages displayed low efferocytic activity, which was significantly enhanced by RvD5 treatment, as evidenced by an increased engulfment of apoptotic neutrophils (**Figure S9A**). This improvement was accompanied by an upregulation of MerTK, a major efferocytic receptor[32], following RvD5 treatment (**Figure S9B**), along with an increased release of the anti-inflammatory cytokine IL-10 (**Figure S9C**). In contrast, the expression levels of other efferocytosis receptors, such as CD14[33] and the scavenger receptor CD36[34], remained unchanged between M1 macrophages and RvD5-treated M1 cells (**Figure S9D**).

Then, we examined the capacity of M1 macrophages to engulf viable Mtb. There was no significant change in the initial bacterial uptake by RvD5-treated

M1 macrophages compared to untreated cells (**Figure 5A**). However, RvD5 treatment lowers IL-1β secretion by M1 macrophages in response to Mtb infection and impaired strongly their microbicidal activity (**Figure 5B-C)**. Additionally, RvD5 prevented the induction of autophagy in Mtb-infected macrophages (**Figure 5D)**, a key mechanism through which macrophages control bacterial growth[35]. Consistent with the autophagy-dependent mycobacterial degradation in enhancing antigen presentation to T cells[36,37], we observed reduced CD4 T cell activation in antigen-presenting cell (APC)-dependent responses against irradiated Mtb (iMtb) when RvD5 was added to the cocultures (**Figure S10A-D**). Of note, this effect was absent in APC-independent T cell activation (**Figure S10E-G**), providing additional evidence that RvD5 compromises macrophage functionality.

Altogether, our results indicate that the omega-3-derived lipid mediator RvD5 reprograms the proinflammatory profile of M1 macrophages toward a more pro-resolving, immunomodulatory phenotype.

HIF1α stabilization restores M1 macrophage features inhibited by the GPR32-RvD5 axis

To investigate whether the inhibition of HIF1α mediates the inhibition of the microbicidal activity of M1 macrophages induced by the -RvD5-GPR32, we stabilized HIF1α expression by using Dimethyloxalylglycine (DMOG). Remarkably, HIF1α stabilization in RvD5-treated M1 macrophages restored their impaired lactate and IL-1β release (**Figure 6A-B**), as well as their microbicidal activity, evidenced by reduced bacillary loads and a higher localization of Mtb in compartments marked by the late endosomal marker, LAMP2 (**Figure 6C-D)**. Interestingly, RvD5-induced pro-resolution features, such as enhanced efferocytic capacity, upregulated MerTK expression, and increased IL-10 production, were diminished following DMOG treatment (**Figure S11A-C**). These findings highlight that the RvD5-GPR32-HIF1α axis suppresses macrophage microbicidal functions and increases susceptibility to Mtb. Importantly, these effects can be reversed through pharmacological stabilization of HIF1α.

Discussion

Pleural TB presents unique challenges for healthcare providers, particularly concerning its treatment. Effective host defense against TB involves the infiltration of peripheral blood cells into the pleural space, resulting in an accumulation of immune cells and soluble factors, including lipid mediators, in tuberculous pleural fluid. SPMs play a critical role in limiting inflammation and preventing collateral damage to healthy tissues. However, it is essential to carefully regulate the potential adverse effects of SPMs on the microbicidal functions of inflammatory macrophages to achieve a balanced approach that supports effective pathogen clearance while minimizing excessive inflammation. While previous studies have highlighted the beneficial roles of SPMs in enhancing the microbicidal activities of macrophages and neutrophils[21,38–40], our study is the first to establish the involvement of the RvD5-GPR32-HIF1α axis in TB. We demonstrate that RvD5, present in pleural TB, activates GPR32, leading to the inhibition of HIF1α-dependent microbicidal activity in macrophages.

Our study centers on two pivotal findings. First, we identified the RvD5-GPR32 axis as a key mediator in the suppression of macrophage glycolysis in pleural effusions. We demonstrated that RvD5 is not only present in pleural effusions but can also be produced by monocytes exposed to the acellular fraction of these effusions. Notably, $CD14^+$ cells in the pleural cavity constitute the primary mononuclear cell population responsible for local production of SPMs, such as resolvins. The accumulation of RvD5 within the pleural cavity correlates with reduced glycolytic capacity in $CD14^+$ cells compared to their circulating counterparts. This suggests that upon entering the pleural cavity, phagocytes undergo a metabolic shift characterized by attenuated glycolytic activity, influenced by the local microenvironment. In line with this, in-vitro exposure of macrophages to RvD5 led to a similar reduction in glycolysis.

We show that pleural macrophages from TB patients undergoing antibiotic treatment exhibit a significant increase in glycolytic activity compared to those from untreated patients. This observation indicates the presence of active mechanisms within the pleural cavity that suppress long-term protective

immune responses, likely modulated by SPMs. Such findings offer a potential explanation for the frequent relapses observed in untreated pleural TB patients, suggesting that while glycolysis in macrophages is locally suppressed during active disease, systemically monocytes in TB patients maintain a dysregulated glycolytic profile, as we recently reported[22]. This dichotomy supports the notion of contrasting metabolic environments at local and systemic levels. Even though using drugs that alter metabolism in all cells might have deleterious implications for patients, and identifying strategies to do so selectively in macrophages has important clinical implications. We propose that upon entering the pleural cavity, monocytes upregulate ALOX5 transcript levels, secrete SPMs, and transition into a state of reduced glycolytic activity. This immunosuppressive metabolic state, however, appears to be reversible with TB treatment, emphasizing the dynamic interplay between local immune modulation and systemic immune dysregulation in pleural TB.

Several studies have identified associations between ALOX5 polymorphisms and increased susceptibility to TB[41,42] or the development of multisystem TB[43]. These studies primarily focus on the role of ALOX5 in synthesizing pro-inflammatory lipid mediators, such as leukotrienes. In contrast, our findings identify RvD5 as a novel and underappreciated player in this context. Supporting our observations, ALOX5-deficient mice have been shown to exhibit increased resistance to Mtb infection[44]. Interestingly, ALOX5 expression has been implicated in both pro-inflammatory and immunosuppressive outcomes across various pathological contexts. For example, in rheumatoid arthritis, increased ALOX5 expression has been associated with harmful inflammation by driving pyroptosis in $CD4^+$ T cells[45]. Conversely, in gliomas, ALOX5 promotes an immunosuppressive phenotype by facilitating M2 polarization in macrophages[46]. These diverse outcomes likely arise from a diverse array of products that ALOX5 can generate, depending on substrate availability. Indeed, ALOX5 can metabolize arachidonic acid, EPA, or DHA to produce oxylipins with distinct biological functions, including 5-HETE, lipoxins, and resolvins[47]. This substrate-driven variability highlights the complexity of ALOX5's involvement in TB and other diseases. It suggests that its effects may change depending on microenvironmental factors, such as lipid availability, cellular metabolic states,

and the balance between pro-inflammatory and pro-resolving mediators. Understanding these dynamics is critical for fully elucidating the dual roles of ALOX5 and for considering therapeutic strategies that target its metabolic pathways in TB and beyond, and inhibition of ALOX5 might have undesired effects due to its pleiotropic function. On the positive side, GPR32 belongs to the most intensively studied drug target family, largely because of their substantial involvement in human pathophysiology and their pharmacological tractability[48].

Controlling excessive inflammation in the pleural space is crucial to prevent tissue damage and maintain host-pathogen balance. While RvD5 has been shown to impair the microbicidal functions of macrophages, other SPMs prevalent in pleural TB, such as PDx and MaR1, do not exhibit these detrimental effects[21]. This underscores an opportunity to selectively enhance SPMs that preserve microbicidal activity while minimizing tissue damage, avoiding those like RvD5. For instance, in tuberculous meningitis, elevated concentrations of SPMs in cerebrospinal fluid have been associated with improved patient survival[49]. These results support the idea of targeted interventions to harness the benefits of SPMs while mitigating the risks.

The literature extensively explores the balance between “proinflammatory” and “protective” lipid mediators, often manipulated through dietary supplementation with omega-3 fatty acids (n-3 PUFAs, precursors of protective lipids) versus omega-6 fatty acids (n-6 PUFAs, mostly precursors of proinflammatory lipids). However, many studies lack a detailed examination of the mechanisms of action for individual lipids. The outcomes of such supplementation studies have been inconsistent, ranging from detrimental effects, such as the impairment of murine macrophage responses to Mtb with omega-3 supplementation[50,51], to beneficial outcomes where n-3 PUFAs enhance immune responses against Mtb[50,52]. These conflicting findings reflect the strong necessity for further research to delineate the specific roles and mechanisms of individual lipid mediators in the context of TB.

Although some reports propose that certain SPMs, such as RvD1[53] or MaR1[54], can enhance cellular respiration in neutrophils and macrophages, our findings did not demonstrate that RvD5 increases absolute mitochondrial respiration in macrophages stimulated with LPS and IFNγ. This discrepancy may be due to the strong metabolic imprinting induced by LPS and IFNγ, which results in decreased OXPHOS that RvD5 cannot counteract. Alternatively, the effect of RvD5 may be limited to reducing glycolysis without activating compensatory energetic mechanisms. These insights further support the complex and context-dependent nature of SPM-mediated metabolic regulation, warranting more in-depth studies to fully understand their roles and therapeutic potential in TB.

Our second key finding reveals that activation of GPR32 by RvD5 inhibits HIF1α-dependent microbicidal activity in macrophages, shedding light on a critical pathway that modulates immune responses in TB. Previously, we demonstrated that lipids extracted from the acellular fraction of TB pleural effusions suppress HIF1α expression, leading to reduced glycolytic and microbicidal phenotypes in macrophages[15]. The present study goes beyond our previous results, as we now show that RvD5 specifically is a major lipid mediator driving this effect through GPR32 binding. While GPR32 is the best characterized receptor for RvD5, it has also been reported that RvD5 can activate GPR101, which is expressed in macrophages[55]. Yet, the potential involvement of this alternative receptor in the observed effects was not explored in this study, leaving an open avenue for future research.

Our results demonstrate that RvD5 impairs Mtb clearance, at least partially, by limiting the induction of autophagy in infected macrophages. Importantly, this suppression of autophagy could be reversed by stabilizing HIF1α, consistent with previous findings that HIF1α promotes autophagy in cancer cells[56]. Additionally, it has been shown that Mtb can inhibit IFNγ-induced autophagy via ALOX5-dependent induction of the Mir155-Mir31-WNT-SHH signaling pathway, which is further supported by findings indicating that pharmacological perturbation of ALOX5 leads to improved control of mycobacterial intracellular loads[57]. However, the role of RvD5 specifically was not investigated in that

study. Interestingly, unlike RvD5, other resolvins such as RvD1 have been reported to promote autophagy in various contexts[58,59]. These findings emphasize the functional specificity of different SPMs and caution against generalizing biological functions across the resolvin family.

Although this study focused primarily on pleural TB, we also identified some GPR32^{+} macrophages located within lung granulomas of infected NHPs. This observation suggests broader implications for the role of the RvD5-GPR32-HIF1α axis in various forms of TB and beyond the pleural cavity. Nevertheless, advancing physiologically relevant studies on this axis remains challenging, as GPR32 is a pseudogene in mice and rats, limiting the use of traditional animal models for further investigation. To address these limitations, experimental approaches have been developed, including a transgenic mouse model expressing human GPR32, which has already been used to investigate its role in atherosclerosis[60]. Additionally, human organoid models provide a more physiologically relevant alternative to classical cell culture systems, enabling a deeper exploration of GPR32 function in a human context[61]. Given these complementary models, further research on GPR32's role in TB control could be highly valuable. In regions with high exposure risk, or where TB prevalence is significant, modulating GPR32 signaling may offer a promising strategy to enhance innate immunity and prevent disease progression.

In conclusion, our study provides valuable insights into the pathophysiology of pleural TB by uncovering RvD5 as a critical lipid mediator that modulates macrophage metabolism and function through GPR32. This work underlines the importance of understanding the specific mechanisms by which lipid mediators influence immune cell metabolism and TB severity. These results may pave the way for developing targeted therapeutic strategies that aim to balance immune regulation, preserve microbicidal activity, and mitigate the detrimental effects of excessive inflammation in TB.

Acknowledgements

We thank the staff of the Regional Center of Hemotherapy of the Garrahan Hospital (Buenos Aires). We thank MetaToul (Toulouse metabolomics & fluxomics facilities, https://mth-metatoul.com/) which is part of the French National Infrastructure for Metabolomics and Fluxomics MetaboHUB-ANR-11-INBS-0010 doi.org/10.15454/VRJK-KY76. We also thank Life Science Editors for editing services (www.lifescienceeditors.com).

This work was supported by the Argentinean National Agency of Promotion of Science and Technology (PICT-2019-01044 and PICT-2020-00501 to LB); the Argentinean National Council of Scientific and Technical Investigations (CONICET, PIP 11220200100299CO to LB); the ICGEB CRP/ARG23-02 Research Grant to LB; Fondation Bettencourt Schueller (EXPORE-TB grant to ON); MSDAVENIR (the FIGHT-TB grant to ON); and the French ANR JCJC-Epic-SCENITH ANR-20-CE14-0028 and CoPoC Inserm-transfert MAT-PI-17493-A-04 to RA.

Author contributions

Conceptualization: CV, GLV and LB. Methodology: JB and LB. Investigation: JB, MMaio, EB, NF, SM, JLMF, AM, FS, FF, TMG, MMatteo, EL, CV, GLV and LB. Resources: AJE, XA, MSC, DP, MO, RA, RKN, ON, CV, GLV, and LB. Formal Analysis: JB, MML, EL, and LB. Writing: JB, MML, EL, ON, CV, GLV, and LB. Visualization: JB, FF, AM, CV, and LB. Supervision: EL, CV, GLV, and LB. Project Administration: LB. Funding acquisition: RA, ON, and LB. Corresponding author: LB is responsible for ownership and responsibility that are inherent to aspects of this study.

Declaration of interests

The authors declare no competing interests.

References

Koeken, V.A.C.M., Verrall, A.J., Netea, M.G., Hill, P.C., and van Crevel, R. (2019). Trained innate immunity and resistance to Mycobacterium tuberculosis infection. Clinical Microbiology and Infection *25*, 1468–1472. https://doi.org/10.1016/J.CMI.2019.02.015.

Biswas, S.K., and Mantovani, A. (2012). Orchestration of metabolism by macrophages. Cell Metab. 2012 Apr 4;15(4):432-7. doi: 10.1016/j.cmet.2011.11.013.

O'Neill, L.A.J., Kishton, R.J., and Rathmell, J. (2016). A guide to immunometabolism for immunologists. Nat Rev Immunol *16*, 553–565. https://doi.org/10.1038/nri.2016.70.

Che, N., Ma, Y., Ruan, H., Xu, L., Wang, X., Yang, X., and Liu, X. (2018). Integrated semi-targeted metabolomics analysis reveals distinct metabolic dysregulation in pleural effusion caused by tuberculosis and malignancy. Clinica Chimica Acta *477*, 81–88. https://doi.org/10.1016/J.CCA.2017.12.003.

Seibert, A.F., Haynes, J., Middleton, R., and Bass, J.B. (1991). Tuberculous pleural effusion; Twenty-year experience. CHEST, Volume 99, Issue 4, 883 – 886. https://doi.org/10.1378/chest.99.4.883.

Sharma, S.K., Mohan, A., and Kohli, M. (2021). Extrapulmonary tuberculosis. Expert Rev Respir Med *15*, 931–948. https://doi.org/10.1080/17476348.2021.1927718.

Macías, A., Sánchez-Montalvá, A., Salvador, F., Villar, A., Tórtola, T., Saborit, N., and Molina, I. (2019). Epidemiology and diagnosis of pleural tuberculosis in a low incidence country with high rate of immigrant population: A retrospective study. International Journal of Infectious Diseases *78*, 34–38. https://doi.org/10.1016/j.ijid.2018.10.005.

Kim, H.J., Lee, H.J., Kwon, S.Y., Yoon, H. Il, Chung, H.S., Lee, C.T., Han, S.K., Shim, Y.S., and Yim, J.J. (2006). The prevalence of pulmonary parenchymal tuberculosis in patients with tuberculous pleuritis. Chest *129*, 1253–1258. https://doi.org/10.1378/chest.129.5.1253.

Sharma, S.K., Mitra, D.K., Balamurugan, A., Pandey, R.M., and Mehra, N.K. (2002). Cytokine polarization in miliary and pleural tuberculosis. J Clin Immunol *22*, 345–352. https://doi.org/10.1023/A:1020604331886/METRICS.

Light, R.W. (2010). Update on tuberculous pleural effusion. Respirology. 2010 Apr;15(3):451-8. doi: 10.1111/j.1440-1843.2010.01723.x.

Genoula, M., Franco, J.L.M., Dupont, M., Kviatcovsky, D., Milillo, A., Schierloh, P., Moraña, E.J., Poggi, S., Palmero, D., Mata-Espinosa, D., et al. (2018). Formation of foamy macrophages by tuberculous pleural effusions is triggered by the interleukin-10/signal transducer and activator of transcription 3 axis through ACAT upregulation. Front Immunol. https://doi.org/10.3389/fimmu.2018.00459.

Lastrucci, C., Bénard, A., Balboa, L., Pingris, K., Souriant, S., Poincloux, R., Al Saati, T., Rasolofo, V., González-Montaner, P., Inwentarz, S., et al. (2015). Tuberculosis is associated with expansion of a motile, permissive and immunomodulatory CD16+ monocyte population via the IL-10/STAT3 axis. Cell Res. https://doi.org/10.1038/cr.2015.123.

Souriant, S., Balboa, L., Dupont, M., Pingris, K., Kviatcovsky, D., Cougoule, C., Lastrucci, C., Bah, A., Gasser, R., Poincloux, R., et al. (2019). Tuberculosis Exacerbates HIV-1 Infection through IL-10/STAT3-Dependent Tunneling Nanotube Formation in Macrophages. Cell Rep. https://doi.org/10.1016/j.celrep.2019.02.091.

Genoula, M., Marín Franco, J.L., Maio, M., Dolotowicz, B., Ferreyra, M., Milillo, M.A., Mascarau, R., Moraña, E.J., Palmero, D., Matteo, M., et al. (2020). Fatty acid oxidation of alternatively activated macrophages prevents foam cell formation, but

Mycobacterium tuberculosis counteracts this process via HIF-1α activation. PLoS Pathog *16*, e1008929. https://doi.org/10.1371/journal.ppat.1008929.

Marín Franco, J.L., Genoula, M., Corral, D., Duette, G., Ferreyra, M., Maio, M., Dolotowicz, M.B., Aparicio-Trejo, O.E., Patiño-Martínez, E., Charton, A., et al. (2020). Host-Derived Lipids from Tuberculous Pleurisy Impair Macrophage Microbicidal-Associated Metabolic Activity. Cell Rep. https://doi.org/10.1016/j.celrep.2020.108547.

Serhan, C.N. (2014). Pro-resolving lipid mediators are leads for resolution physiology. Nature *510*, 92–101. https://doi.org/10.1038/NATURE13479.

Centanni, D., Henricks, P.A.J., and Engels, F. (2023). The therapeutic potential of resolvins in pulmonary diseases. Eur J Pharmacol *958*, 176047. https://doi.org/10.1016/J.EJPHAR.2023.176047.

Dalli, J., Winkler, J.W., Colas, R.A., Arnardottir, H., Cheng, C.Y.C., Chiang, N., Petasis, N.A., and Serhan, C.N. (2013). Resolvin D3 and Aspirin-Triggered Resolvin D3 Are Potent Immunoresolvents. Chem Biol *20*, 188. https://doi.org/10.1016/J.CHEMBIOL.2012.11.010.

Krishnamoorthy, S., Recchiuti, A., Chiang, N., Yacoubian, S., Lee, C.H., Yang, R., Petasis, N.A., and Serhan, C.N. (2010). Resolvin D1 binds human phagocytes with evidence for proresolving receptors. Proc Natl Acad Sci U S A *107*, 1660–1665. https://doi.org/10.1073/PNAS.0907342107/SUPPL_FILE/PNAS.200907342SI.PDF.

Chiang, N., Fredman, G., Bäckhed, F., Oh, S.F., Vickery, T., Schmidt, B.A., and Serhan, C.N. (2012). Infection regulates pro-resolving mediators that lower antibiotic requirements. Nature 2012 484:7395 *484*, 524–528. https://doi.org/10.1038/nature11042.

Ruiz, A., Sarabia, C., Torres, M., and Juárez, E. (2019). Resolvin D1 (RvD1) and maresin 1 (Mar1) contribute to human macrophage control of M. tuberculosis infection while resolving inflammation. Int Immunopharmacol *74*. https://doi.org/10.1016/J.INTIMP.2019.105694.

Maio, M., Barros, J., Joly, M., Vahlas, Z., Franco, J.L.M., Genoula, M., Monard, S., Vecchione, M.B., Fuentes, F., Polo, V.G., et al. (2024). Elevated glycolytic metabolism of monocytes limits the generation of HIF-1α-driven migratory dendritic cells in tuberculosis. Elife *12*. https://doi.org/10.7554/ELIFE.89319.3.

Argüello, R.J., Combes, A.J., Char, R., Gigan, J.P., Baaziz, A.I., Bousiquot, E., Camosseto, V., Samad, B., Tsui, J., Yan, P., et al. (2020). SCENITH: A Flow Cytometry-Based Method to Functionally Profile Energy Metabolism with Single-Cell Resolution. Cell Metab. https://doi.org/10.1016/j.cmet.2020.11.007.

Cai, Y., Wang, Y., Shi, C., Dai, Y., Li, F., Xu, Y., Zhang, P., Kong, F., Deng, G., Wen, Z., et al. (2022). Single-cell immune profiling reveals functional diversity of T cells in tuberculous pleural effusion. Journal of Experimental Medicine *219*. https://doi.org/10.1084/JEM.20211777/212978.

Dupont, M., Souriant, S., Balboa, L., Vu Manh, T.-P., Pingris, K., Rousset, S., Cougoule, C., Rombouts, Y., Poincloux, R., Ben Neji, M., et al. (2020). Tuberculosis-associated IFN-I induces Siglec-1 on tunneling nanotubes and favors HIV-1 spread in macrophages. Elife. https://doi.org/10.7554/eLife.52535.

Schebb, N.H., Kühn, H., Kahnt, A.S., Rund, K.M., O'Donnell, V.B., Flamand, N., Peters-Golden, M., Jakobsson, P.J., Weylandt, K.H., Rohwer, N., et al. (2022). Formation, Signaling and Occurrence of Specialized Pro-Resolving Lipid Mediators—What is the Evidence so far? Front Pharmacol *13*. https://doi.org/10.3389/FPHAR.2022.838782/FULL.

Lee, J., Lim, J.K., Yoo, S.S., Lee, S.Y., Cha, S.I., Park, J.Y., and Kim, C.H. (2016). Different characteristics of tuberculous pleural effusion according to pleural fluid

cellular predominance and loculation. J Thorac Dis *8*, 1935–1942. https://doi.org/10.21037/JTD.2016.06.54.

48. Schmid, M., Gemperle, C., Rimann, N., and Hersberger, M. (2016). Resolvin D1 Polarizes Primary Human Macrophages toward a Proresolution Phenotype through GPR32. The Journal of Immunology *196*, 3429–3437. https://doi.org/10.4049/JIMMUNOL.1501701.

49. Palsson-Mcdermott, E.M., Curtis, A.M., Goel, G., Lauterbach, M.A.R., Sheedy, F.J., Gleeson, L.E., Van Den Bosch, M.W.M., Quinn, S.R., Domingo-Fernandez, R., Johnson, D.G.W., et al. (2015). Pyruvate kinase M2 regulates hif-1α activity and il-1β induction and is a critical determinant of the warburg effect in LPS-activated macrophages. Cell Metab. https://doi.org/10.1016/j.cmet.2014.12.005.

50. Park, J., Langmead, C.J., and Riddy, D.M. (2020). New Advances in Targeting the Resolution of Inflammation: Implications for Specialized Pro-Resolving Mediator GPCR Drug Discovery. ACS Pharmacol Transl Sci *3*, 88. https://doi.org/10.1021/ACSPTSCI.9B00075.

51. Viola, A., Munari, F., Sánchez-Rodríguez, R., Scolaro, T., and Castegna, A. (2019). The metabolic signature of macrophage responses. Front Immunol *10*, 466337. https://doi.org/10.3389/FIMMU.2019.01462/BIBTEX.

52. Scott, R.S., McMahon, E.J., Pop, S.M., Reap, E.A., Caricchio, R., Cohen, P.L., Shelton Earp, H., and Matsushima, G.K. (2001). Phagocytosis and clearance of apoptotic cells is mediated by MER. Nature *411*, 207–211. https://doi.org/10.1038/35075603.

53. Devitt, A., Moffatt, O.D., Raykundalia, C., Capra, J.D., Simmons, D.L., and Gregory, C.D. (1998). Human CD14 mediates recognition and phagocytosis of apoptotic cells. Nature 1998 392:6675 *392*, 505–509. https://doi.org/10.1038/33169.

54. Savill, J., Hogg, N., Ren, Y., and Haslett, C. (1992). Thrombospondin cooperates with CD36 and the vitronectin receptor in macrophage recognition of neutrophils undergoing apoptosis. J Clin Invest *90*, 1513–1522. https://doi.org/10.1172/JCI116019.

55. Golovkine, G.R., Roberts, A.W., Morrison, H.M., Rivera-Lugo, R., McCall, R.M., Nilsson, H., Garelis, N.E., Repasy, T., Cronce, M., Budzik, J., et al. (2023). Autophagy restricts Mycobacterium tuberculosis during acute infection in mice. Nature Microbiology 2023 8:5 *8*, 819–832. https://doi.org/10.1038/s41564-023-01354-6.

56. Dang, A.T., Teles, R.M.B., Liu, P.T., Choi, A., Legaspi, A., Sarno, E.N., Ochoa, M.T., Parvatiyar, K., Cheng, G., Gilliet, M., et al. (2019). Autophagy links antimicrobial activity with antigen presentation in Langerhans cells. JCI Insight *4*. https://doi.org/10.1172/JCI.INSIGHT.126955.

57. Jagannath, C., Lindsey, D.R., Dhandayuthapani, S., Xu, Y., Hunter, Jr., R.L., and Eissa, N.T. (2009). Autophagy enhances the efficacy of BCG vaccine by increasing peptide presentation in mouse dendritic cells. Nat Med *15*, 267–277.

58. Croasdell, A., Lacy, S.H., Thatcher, T.H., Sime, P.J., and Phipps, R.P. (2016). Resolvin D1 Dampens Pulmonary Inflammation and Promotes Clearance of Nontypeable Haemophilus influenzae. J Immunol *196*, 2742–2752. https://doi.org/10.4049/JIMMUNOL.1502331.

59. Wu, B., Capilato, J., Pham, M.P., Walker, J., Spur, B., Rodriguez, A., Perez, L.J., and Yin, K. (2016). Lipoxin A4 augments host defense in sepsis and reduces Pseudomonas aeruginosa virulence through quorum sensing inhibition. FASEB J *30*, 2400–2410. https://doi.org/10.1096/FJ.201500029R.

60. Wu, B., Walker, J., Spur, B., Rodriguez, A., and Yin, K. (2015). Effects of Lipoxin A4 on antimicrobial actions of neutrophils in sepsis. Prostaglandins Leukot Essent Fatty Acids *94*, 55–64. https://doi.org/10.1016/J.PLEFA.2014.11.005.

987. Shen, C., Wu, X.R., Wang, B. Bin, Sun, L., Jiao, W.W., Wang, J., Feng, W.X., Xiao, J., Miao, Q., Liu, F., et al. (2013). ALOX5 is associated with tuberculosis in a subset of the pediatric population of North China. Genet Test Mol Biomarkers *17*, 284–288. https://doi.org/10.1089/GTMB.2012.0426.
991. Herb, F., Thye, T., Niemann, S., Browne, E.N.L., Chinbuah, M.A., Gyapong, J., Osei, I., Owusu-Dabo, E., Werz, O., Rüsch-Gerdes, S., et al. (2008). ALOX5 variants associated with susceptibility to human pulmonary tuberculosis. Hum Mol Genet *17*, 1052–1060. https://doi.org/10.1093/HMG/DDM378.
995. Zhang, J., Wang, M. gui, and He, J.Q. (2023). Association between a single nucleotide polymorphism of the ALOX5 gene and susceptibility to multisystem tuberculosis in a Chinese Han population. Microb Pathog *183*. https://doi.org/10.1016/J.MICPATH.2023.106289.
999. Bafica, A., Scanga, C.A., Serhan, C., Machado, F., White, S., Sher, A., and Aliberti, J. (2005). Host control of Mycobacterium tuberculosis is regulated by 5-lipoxygenase-dependent lipoxin production. Journal of Clinical Investigation. https://doi.org/10.1172/JCI23949.
1003. Cai, H., Zhang, J., Xu, H., Sun, W., Wu, W., Dong, C., Zhou, P., Xue, C., Nan, Y., Ni, Y., et al. (2024). ALOX5 drives the pyroptosis of CD4+ T cells and tissue inflammation in rheumatoid arthritis. Sci Signal *17*. https://doi.org/10.1126/SCISIGNAL.ADH1178/SUPPL_FILE/SCISIGNAL.ADH1178_MDAR_REPRODUCIBILITY_CHECKLIST.PDF.
1008. Chen, T., Liu, J., Wang, C., Wang, Z., Zhou, J., Lin, J., Mao, J., Pan, T., Wang, J., Xu, H., et al. (2024). ALOX5 contributes to glioma progression by promoting 5-HETE-mediated immunosuppressive M2 polarization and PD-L1 expression of glioma-associated microglia/macrophages. J Immunother Cancer *12*, e009492. https://doi.org/10.1136/JITC-2024-009492.
1013. Kahnt, A.S., Häfner, A.K., and Steinhilber, D. (2024). The role of human 5-Lipoxygenase (5-LO) in carcinogenesis - a question of canonical and non-canonical functions. Oncogene 2024 43:18 *43*, 1319–1327. https://doi.org/10.1038/s41388-024-03016-1.
1017. Hauser, A.S., Attwood, M.M., Rask-Andersen, M., Schiöth, H.B., and Gloriam, D.E. (2017). Trends in GPCR drug discovery: new agents, targets and indications. Nat Rev Drug Discov *16*, 829. https://doi.org/10.1038/NRD.2017.178.
1020. Colas, R.A., Nhat, L.T.H., Thuong, N.T.T., Gómez, E.A., Ly, L., Thanh, H.H., Mai, N.T.H., Phu, N.H., Thwaites, G.E., and Dalli, J. (2019). Proresolving mediator profiles in cerebrospinal fluid are linked with disease severity and outcome in adults with tuberculous meningitis. FASEB J *33*, 13028–13039. https://doi.org/10.1096/FJ.201901590R.
1025. Jordao, L., Lengeling, A., Bordat, Y., Boudou, F., Gicquel, B., Neyrolles, O., Becker, P.D., Guzman, C.A., Griffiths, G., and Anes, E. (2008). Effects of omega-3 and -6 fatty acids on Mycobacterium tuberculosis in macrophages and in mice. Microbes Infect *10*, 1379–1386. https://doi.org/10.1016/J.MICINF.2008.08.004.
1029. Bonilla, D.L., Ly, L.H., Fan, Y.Y., Chapkin, R.S., and Mcmurray, D.N. (2010). Incorporation of a Dietary Omega 3 Fatty Acid Impairs Murine Macrophage Responses to Mycobacterium tuberculosis. PLoS One *5*, e10878. https://doi.org/10.1371/JOURNAL.PONE.0010878.
1032. Nienaber, A., Baumgartner, J., Dolman, R.C., Ozturk, M., Zandberg, L., Hayford, F.E.A., Brombacher, F., Blaauw, R., Parihar, S.P., Smuts, C.M., et al. (2020). Omega-3 Fatty Acid and Iron Supplementation Alone, but Not in Combination, Lower

Inflammation and Anemia of Infection in Mycobacterium tuberculosis-Infected Mice. Nutrients *12*, 1–22. https://doi.org/10.3390/NU12092897.

Li, L., Cheng, S.Q., Sun, Y.Q., Yu, J.B., Huang, X.X., Dong, Y.F., Ji, J., Zhang, X.Y., Hu, G., and Sun, X.L. (2023). Resolvin D1 reprograms energy metabolism to promote microglia to phagocytize neutrophils after ischemic stroke. Cell Rep *42*. https://doi.org/10.1016/J.CELREP.2023.112617.

Calderin, E.P., McNally, L., Hill, B.G., and Hellmann, J. (2021). Specialized pro-resolving lipid mediators stimulate mitochondrial metabolism in macrophages. The Journal of Immunology *206*, 97.09-97.09. https://doi.org/10.4049/JIMMUNOL.206.SUPP.97.09.

Chiang, N., and Serha, C.N. (2020). Specialized pro-resolving mediator network: an update on production and actions. Essays Biochem *64*, 443–462. https://doi.org/10.1042/EBC20200018.

Wang, P., Long, M., Zhang, S., Cheng, Z., Zhao, X., He, F., Liu, H., and Ming, L. (2017). Hypoxia inducible factor-1α regulates autophagy via the p27-E2F1 signaling pathway. Mol Med Rep *16*, 2107. https://doi.org/10.3892/MMR.2017.6794.

Holla, S., Kurowska-Stolarska, M., Bayry, J., and Balaji, K.N. (2013). Selective inhibition of IFNG-induced autophagy by Mir155- and Mir31-responsive WNT5A and SHH signaling. Autophagy *10*, 311. https://doi.org/10.4161/AUTO.27225.

Prieto, P., Rosales-Mendoza, C.E., Terron, V., Toledano, V., Cuadrado, A., López-Collazo, E., Bannenberg, G., Martín-Sanz, P., Fernández-Velasco, M., and Boscá, L. (2015). Activation of autophagy in macrophages by pro-resolving lipid mediators. Autophagy *11*, 1729–1744. https://doi.org/10.1080/15548627.2015.1078958.

Xiong, W., Wang, H., Zhang, H., Xing, Y., Gao, W., Chen, L., Chen, L., and Dai, Z. (2023). Resolvin D1 attenuates depressive-like behavior in LPS-challenged mice by promoting microglial autophagy. Inflammopharmacology *31*, 2061–2075. https://doi.org/10.1007/S10787-023-01234-9.

Arnardottir, H., Thul, S., Pawelzik, S.C., Karadimou, G., Artiach, G., Gallina, A.L., Mysdotter, V., Carracedo, M., Tarnawski, L., Caravaca, A.S., et al. (2021). The resolvin D1 receptor GPR32 transduces inflammation resolution and atheroprotection. J Clin Invest *131*. https://doi.org/10.1172/JCI142883.

Beumer, J., Geurts, M.H., Lamers, M.M., Puschhof, J., Zhang, J., van der Vaart, J., Mykytyn, A.Z., Breugem, T.I., Riesebosch, S., Schipper, D., et al. (2021). A CRISPR/Cas9 genetically engineered organoid biobank reveals essential host factors for coronaviruses. Nat Commun *12*, 5498. https://doi.org/10.1038/S41467-021-25729-7.

Figure Legends

Figure 1. Enrichment in specialized resolution lipid mediators correlates with impaired macrophage glycolysis in tuberculous pleural effusions. (A) M1 Macrophages were exposed to pleural effusions and lactate release was measured. Non-tuberculous (non-TB) samples are represented as follows: black bars indicate cardiac failures, dark gray bars represent pneumonias, and light gray bars denote malignant conditions. Yellow bars correspond to tuberculous (TB) effusions, with dotted bars representing pooled samples and empty bars indicating individual patients. **(B)** Heat map illustrating the relative abundance of lipids detected through lipidomic analysis in pleural effusions classified as TB and non-TB (vs. means ratio) Color code are ratios (0-1). Lipids are grouped by their precursor PUFAs, with a focus on the SPM family. The lipid species with a red border are the ones statistically increased in TB samples. **(C)** The volcano plot depicts fold changes in lipid levels between TB (n=13) and non-TB (n=5) pleural effusion samples against their statistical significance (p-value) for each of the 36 detected metabolites. **(D)** Correlation analysis: Correlations between the inhibition of lactate release induced by pleural effusions and the abundance of specific lipids are shown. Spearman's correlation coefficient (r) and significance levels are reported (**p<0,01; ***p<0,001). LA: linoleic acid, AA: arachidonic acid, DHA: docosahexaenoic acid, EPA: eicosapentaenoic acid; SPM: specialized resolution lipid mediators; PUFA: polyunsaturated fatty acids.

Figure 2. CD14+ cells synthesize RvD5 and its receptor GPR32 in tuberculous pleural effusions. (A) Single cell RNA-seq data visualized through 2D UMAP plot: visualization of mononuclear cells from blood and pleural fluid of TB patients, with cells color-coded by major cell types (PBMC, n=5; PFMC n=5). **(B)** *ALOX5 expression:* Expression levels in various cell lineages, and **(C)** specifically in monocytes from different locations. Statistical analysis was performed using Wilcoxon nonparametric tests, with a significant difference between PFMC (n=5) versus PBMC (n=5) ($p=6x10^{-8}$). **(D)** *RvD5 Determination:* Quantification of RvD5 in monocytes treated in vitro with either PBS 1x or TB-PE (n=6). The proportion of RvD5-producing monocytes out of a total of 6 independent donors is shown above each bar. Statistical analysis was performed using the Fisher's exact test, (**p<0,01). **(E)** Flow cytometry analysis was performed to compare GPR32 expression between CD14+ cells from peripheral blood and pleural effusions. Representative dot plots showing GPR32 expression on $CD14^+$ cells from paired blood and TB pleural mononuclear cells. **(F)** Cell surface expression of GPR32, presented as median fluorescence intensity (MFI) normalized to fluorescence minus one control (MFI/FMO), in paired blood and pleural mononuclear cells from TB (n=3) and a single non-TB patient (n=1). Data are shown as scatter plots, with each circle representing an individual. Means ± SEM are indicated. **(G)** Immunostaining of GPR32: Representative images of lung tissue from Mtb-infected non-human primates with severe pathology. *Left panel*: immunostaining of GPR32 (green: Alexa-488), CD68 (red, Alexa-555), and nuclei (blue, DAPI), (scale bar = 500 µm). *Right panel*: Magnified view of the boxed area in the left panel. Arrows indicate cells positive for GPR32 only (green), CD68 only (red), or both GPR32

and CD68 (yellow) (scale bar = 20 μm). PBMC: peripheral blood mononuclear cells; PFMC: pleural fluid mononuclear cells.

Figure 3. The RvD5-GPR32 axis mediates the inhibition of macrophage glycolysis induced by TB pleural effusions. (A) *Lactate release:* Unstimulated (M0) or LPS and IFNγ-activated (M1) macrophages were treated with RvD5 (33nM), 20% v/v TB-PE (PE), or vehicle (ethanol) for 24h (n=8). **(B)** *HIF1α Expression:* Expression level of HIF1α in M0 or M1 macrophages exposed to RvD5 or ethanol (n=6). **(C)** *RvD5 effect on Mtb-stimulated macrophages:* Lactate release by unstimulated (M0) or IFNγ-activated (M1) macrophages exposed to irradiated Mtb (iMtb) and treated with RvD5 or vehicle (ethanol) after 24h (n=7). Statistical analysis was performed using 2-way ANOVA followed by Dunnett's multiple comparisons test (*p<0.05 vs. M1 Macrophages). RvD5 directly inhibited glycolysis in macrophages. **(D)** GPR32 surface expression: Representative histogram showing GPR32 surface expression as assessed by flow cytometry on human macrophages stimulated with LPS/IFNγ (M1) or unstimulated (Isotype, M0). **(E-F)** Neutralization of GPR32: Macrophages stimulated with LPS/IFNγ (M1) were treated with neutralizing antibodies against GPR32 (aGPR32) before RvD5 or 20% v/v TB-PE (PE) addition. **(E)** Lactate release (n=6) and **(F)** HIF1α expression (n=5) was measured. Horizontal dotted lines indicate mean values for M0 macrophages. The impaired glycolysis detected in macrophages was rescued by GPR32 inhibition. Statistical analysis was performed using 2-way ANOVA followed by Holm-Sidak's multiple comparisons test (*p<0.05; **p<0.01 for presence vs. absence of aGPR32). Data are shown as scatter plots, with each circle representing an individual. Means ± SEM are indicated.

Figure 4. Activation of the RvD5-GPR32 Axis Reduces Glycolysis Without Affecting Mitochondrial Bioenergetics in M1 macrophages. (A) *Basal glycolysis:* Measured in $CD14^+$ cells from blood or pleural fluid of TB and non-TB patients (treated and untreated) using SCENITH. Sample sizes: untreated TB patients (n=5), treated TB patients (n=3), and non-TB patients (n=2). Statistical tests: paired t-test (*p<0.05) for pleural fluid mononuclear cells (PFMC) vs. blood monocytes cells (PBMC) within each group, and Mann-Whitney test (*p<0.05) for treated vs. untreated PFMC. **(B)** *Mitochondrial dependence and glycolytic capacity:* Analyzed in M0, M1 and RvD5-treated M1 macrophages using SCENITH (n=4). **(C)** *Extracellular acidification rate (ECAR):* Measured in M0 and M1 macrophages, treated or not with RvD5 (n=6). Statistical analysis: 2-way ANOVA followed by Tukey's multiple comparisons test (*p<0.05). **(D)** *Oxygen consumption rate (OCR):* Traces and respiration parameters in M0 and M1 macrophages treated or untreated with RvD5 were determined using the Seahorse XF24 Analyzer. Respiratory parameters included basal respiration, ATP-linked respiration, proton leak, maximal respiration, spare respiratory capacity (SRC), and non-mitochondrial respiration. Representative data from one of six experiments are shown, with means ± SEM of six independent donors. Statistical analysis: 2-way ANOVA with the Benjamini, Krieger and Yekutieli two-stage linear step-up procedures (*p < 0.05). **(E)** *ATP production contribution*: Percentages of ATP from mitochondrial oxidative phosphorylation (MitoATP) and glycolysis (GlycoATP) in M0 and M1 macrophages treated or untreated with RvD5 (n=5). Statistical analysis: 1-way ANOVA with Sidak's multiple comparisons test (**p<0.01). **(F)** *ECAR in the*

presence of aGPR32: M1 macrophages treated with RvD5, with or without neutralizing antibodies against GPR32 (aGPR32, n=3). Statistical analysis: paired t-test (*p < 0.05). **(G)** *OCR in the presence of aGPR32*: OCR traces and respiration parameters for RvD5-treated M1 macrophages in the presence or absence of aGPR32 (n=3). Statistical analysis: 2-way ANOVA with Benjamini, Krieger, and Yekutieli procedure (*p<0.05; **p<0.01). **(H)** ATP production contributions in the presence of aGPR32: Percentages of MitoATP and glycoATP in RvD5-treated M1 macrophages in the presence or absence of aGPR32 (n=3). Statistical analysis: paired t-test (***p<0.001). Data are displayed as scatter plots, with each circle representing an individual donor. Means ± SEM are indicated.

Figure 5. RvD5 Impairs Mycobacterial control by M1 Macrophages. (A) *Initial uptake of Mtb*: Unstimulated or M1 (IFNγ-activated) macrophages, treated or untreated with RvD5, were infected with Mtb expressing the red fluorescent protein (RFP). The percentage of Mtb-RFP$^+$ was quantified 4 h post-infection to determine initial uptake. Results are expressed relative to uptake by unstimulated cells (n=4). Statistical analysis: Wilcoxon t-tests comparing M1 macrophages with or without RvD5. **(B)** *IL-1β levels*: Supernatants collected at 24 h post-infection were analyzed by ELISA to measure IL-1β levels (n=9). **(C)** *Mycobacterial growth*: Colony-forming units (CFU) were counted 72 h post-infection in unstimulated or M1 macrophages with and without RvD5 (n=6). Statistical analysis for (B-C): 2-way ANOVA followed by Dunnett's multiple comparisons (*p<0.05; **p<0.01). The data are represented as scatter plots with each circle representing a single individual, means ± SEM are shown. **(D)** *Autophagy in infected macrophages*: Representative micrographs show macrophages infected with Mtb-RFP in the presence or absence of RvD5 for 24 h. Nuclei were stained with DAPI, and the autophagy marker LC3 was visualized via Alexa Fluor 488-conjugated antibodies. The percentage of infected cells (Mtb-RFP$^+$) exhibiting LC3 puncta per field was quantified between M1 macrophages treated or untreated with RvD5. Statistical analysis: Nested t-tests from two independent experiments, including 10 images per condition.

Figure 6. Chemical HIF1α Stabilization Restores RvD5-mediated M1 Macrophage metabolism and function. (A) *Lactate release:* Unstimulated (M0) or LPS and IFNγ-activated (M1) macrophages were treated with RvD5 in the presence or absence of the HIF1α stabilizer, DMOG, for 24 h (n=11). **(B-D)** IFNγ-activated macrophages (M1) treated or not with RvD5, with or without DMOG, were infected with Mtb. **(B)** *IL-1β levels:* Supernatants collected 24 h post-infection were analyzed by ELISA to quantify IL-1β levels (n=8). **(C)** *Mycobacterial growth*: Colony-forming units (CFU) were counted 72 h post-infection (n=6). Statistical analyses (A-C): 2-way ANOVA followed by Dunnett's multiple comparisons test (*p<0.05). Data are represented as scatter plots, with each circle corresponding to an individual donor. Means ± SEM are indicated. **(D)** *Colocalization of Mtb-RFP with LAMP2:* Representative micrographs of macrophages infected with Mtb expressing the red fluorescent protein (Mtb-RFP) for 24 h. Nuclei were stained with DAPI, and the late endosome marker LAMP2 was identified using Alexa Fluor 633-conjugated antibodies. Lower panels show magnified views of the boxed areas (scale bar = 10 μm). Right

panel shows Manders colocalization coefficients reporting the fraction of Mtb that colocalized with LAMP2 staining. Statistical analysis: 1-way ANOVA followed by Tukey's multiple comparisons test (*$p<0.05$), based on 10 images per condition from a representative experiment.

Figure 1

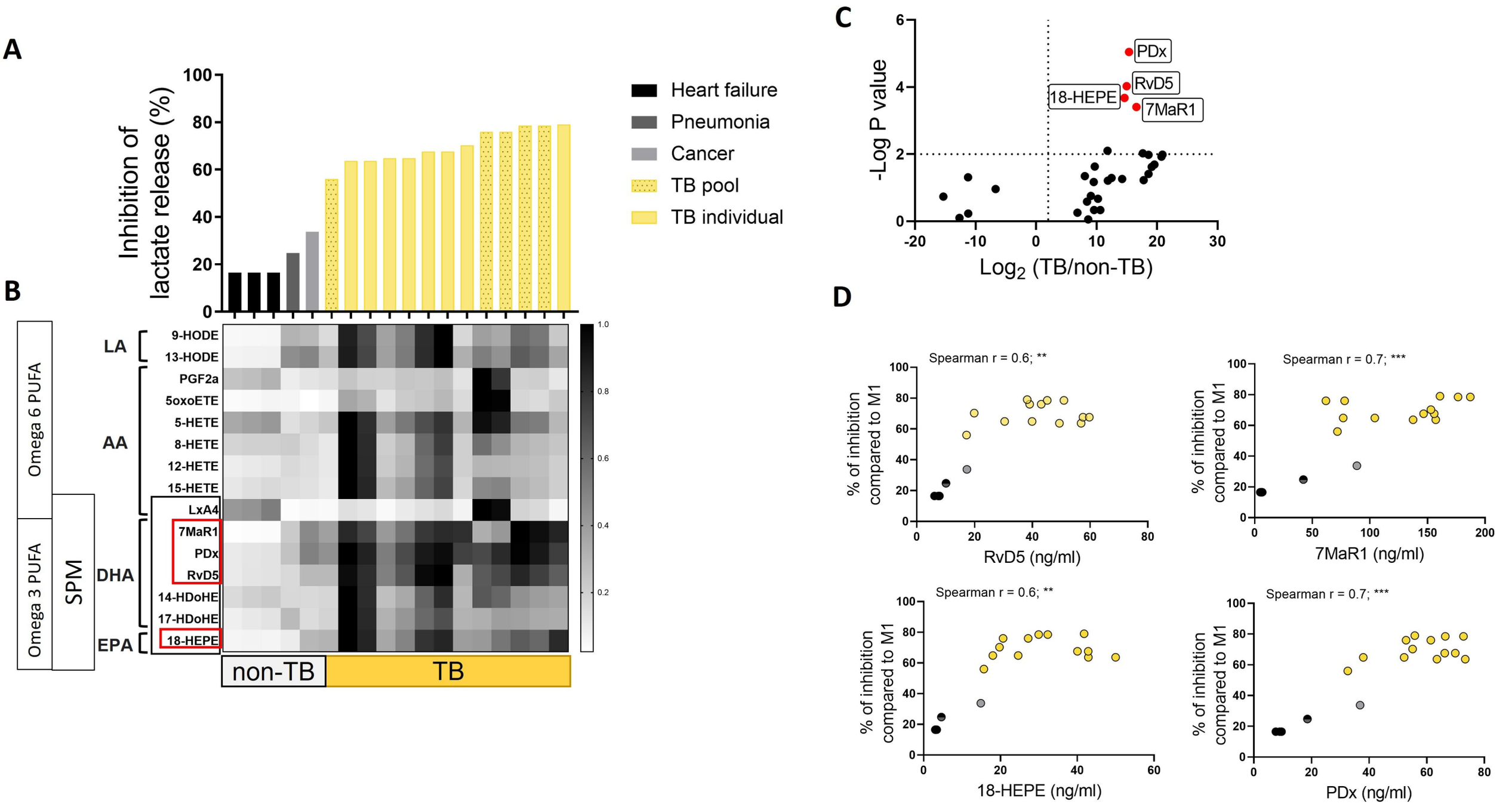
A
Inhibition of lactate release (%)
Heart failure
Pneumonia
Cancer
TB pool
TB individual
B
Omega 6 PUFA
Omega 3 PUFA
SPM
LA
AA
DHA
EPA
9-HODE
13-HODE
PGF2a
5oxoETE
5-HETE
8-HETE
12-HETE
15-HETE
LxA4
7MaR1
PDx
RvD5
14-HDoHE
17-HDoHE
18-HEPE
non-TB
TB
C
-Log P value
Log2 (TB/non-TB)
PDx
RvD5
18-HEPE
7MaR1
D
Spearman r = 0.6; **
Spearman r = 0.7; ***
% of inhibition compared to M1
RvD5 (ng/ml)
7MaR1 (ng/ml)
18-HEPE (ng/ml)
PDx (ng/ml)

Figure 2

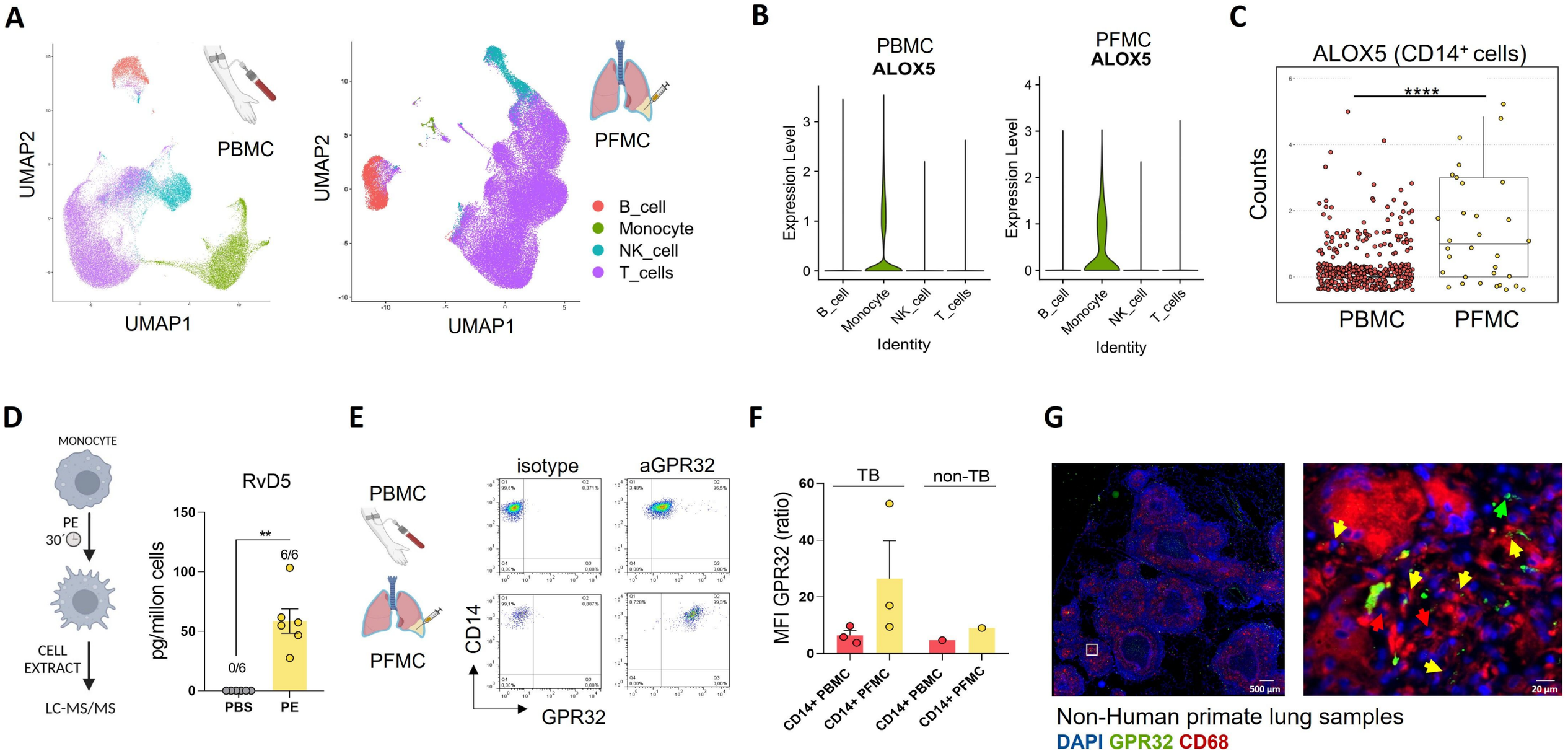
A
UMAP2
UMAP1
PBMC
PFMC
B_cell
Monocyte
NK_cell
T_cells
B
PBMC
ALOX5
PFMC
ALOX5
Expression Level
Identity
C
ALOX5 (CD14+ cells)
Counts
****
PBMC
PFMC
D
MONOCYTE
PE
30´
CELL
EXTRACT
LC-MS/MS
RvD5
pg/millon cells
**
6/6
0/6
PBS
PE
E
PBMC
PFMC
isotype
aGPR32
CD14
GPR32
F
TB
non-TB
MFI GPR32 (ratio)
CD14+ PBMC
CD14+ PFMC
CD14+ PBMC
CD14+ PFMC
G
500 µm
20 µm
Non-Human primate lung samples
DAPI GPR32 CD68

Figure 3

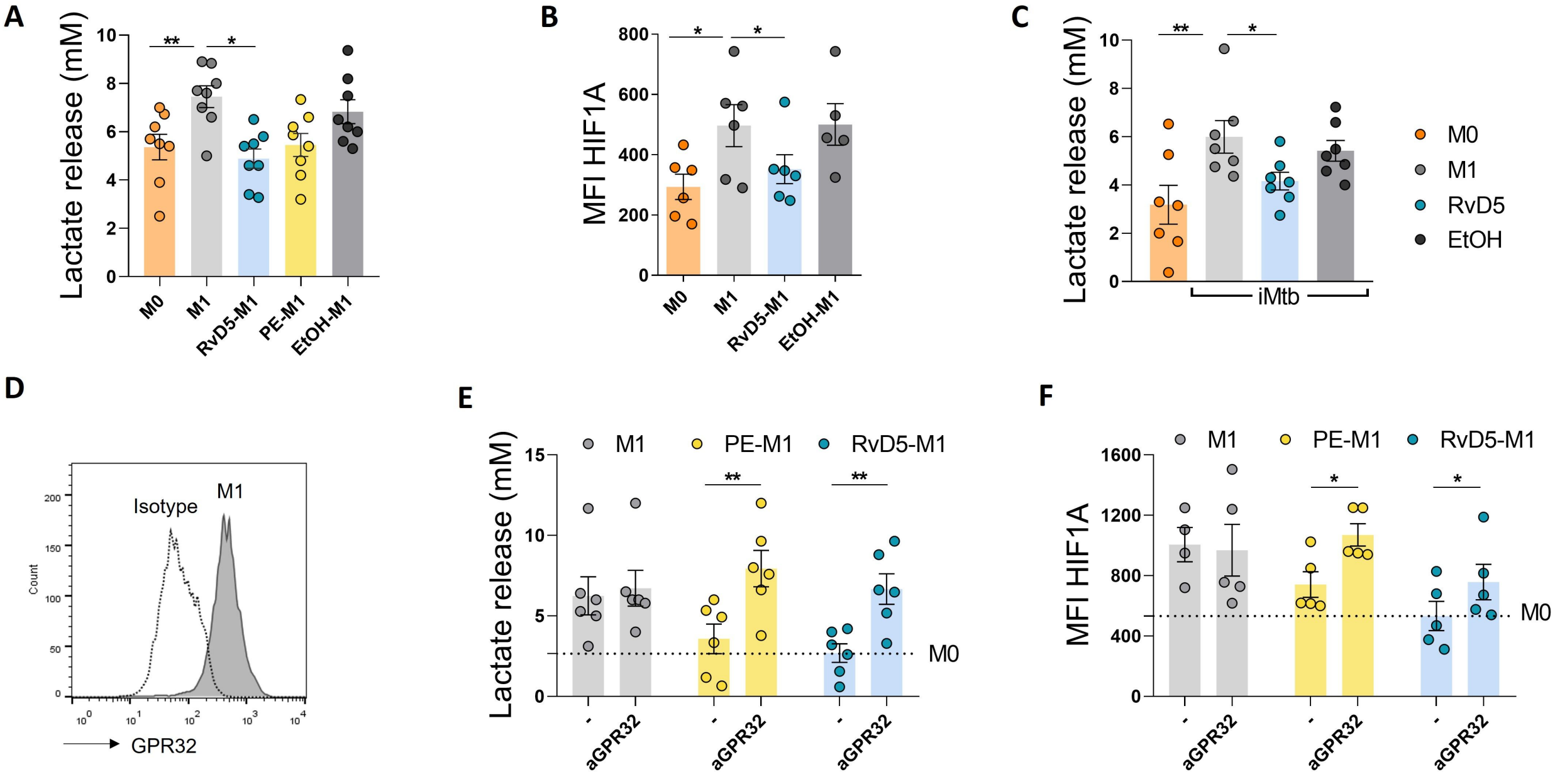
A
Lactate release (mM)
M0
M1
RvD5-M1
PE-M1
EtOH-M1
B
MFI HIF1A
M0
M1
RvD5-M1
EtOH-M1
C
Lactate release (mM)
iMtb
M0
M1
RvD5
EtOH
D
Isotype
M1
Count
GPR32
E
Lactate release (mM)
M1
PE-M1
RvD5-M1
M0
-
aGPR32
F
MFI HIF1A
M1
PE-M1
RvD5-M1
M0
-
aGPR32

Figure 4

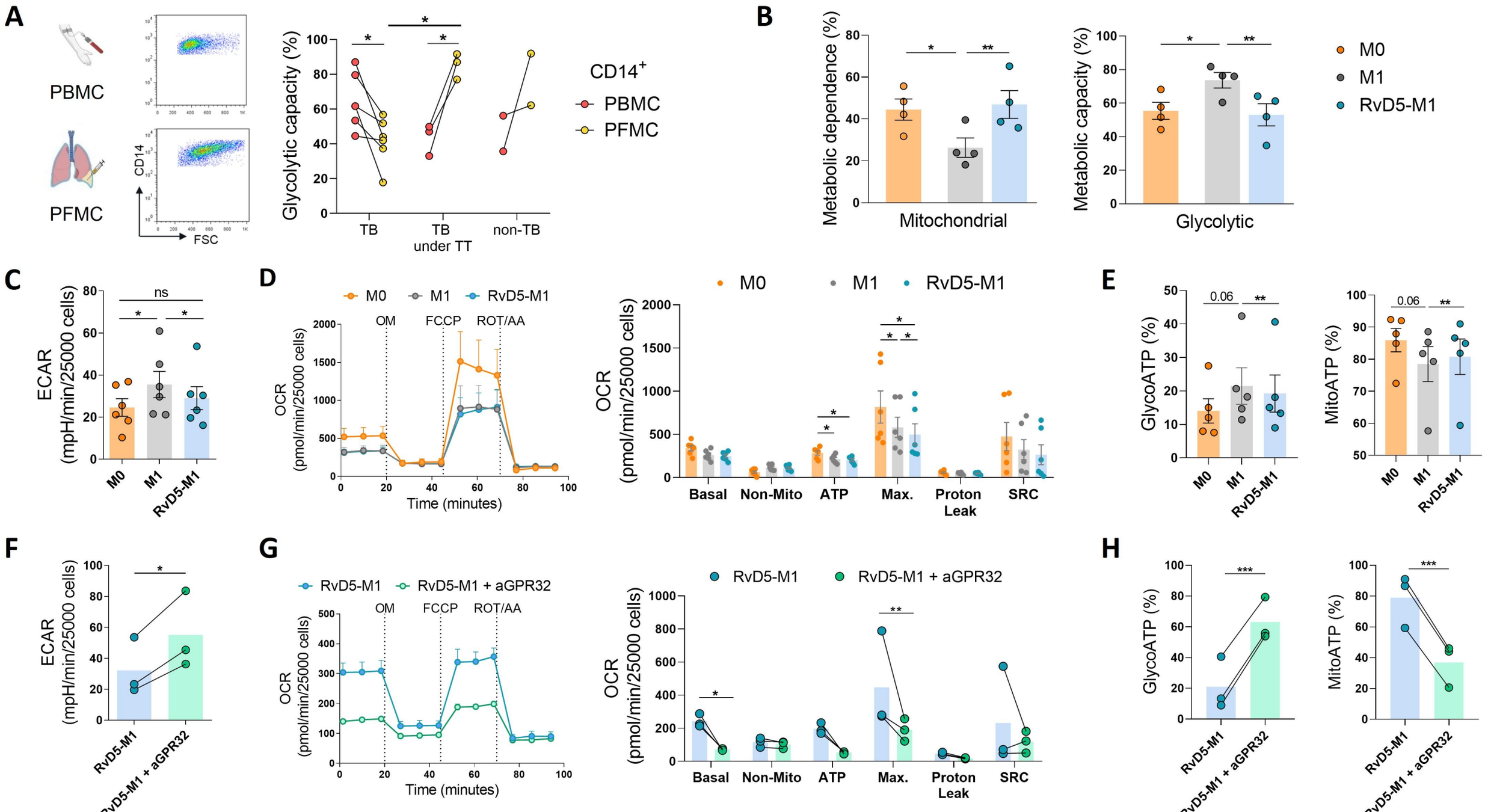
A
PBMC
PFMC
CD14
FSC
Glycolytic capacity (%)
TB
TB under TT
non-TB
CD14+
PBMC
PFMC
B
Metabolic dependence (%)
Mitochondrial
Metabolic capacity (%)
Glycolytic
M0
M1
RvD5-M1
C
ECAR (mpH/min/25000 cells)
ns
M0
M1
RvD5-M1
D
OCR (pmol/min/25000 cells)
OM
FCCP
ROT/AA
Time (minutes)
Basal
Non-Mito
ATP
Max.
Proton Leak
SRC
E
GlycoATP (%)
MitoATP (%)
0.06
F
RvD5-M1
RvD5-M1 + aGPR32
G
H

Figure 5

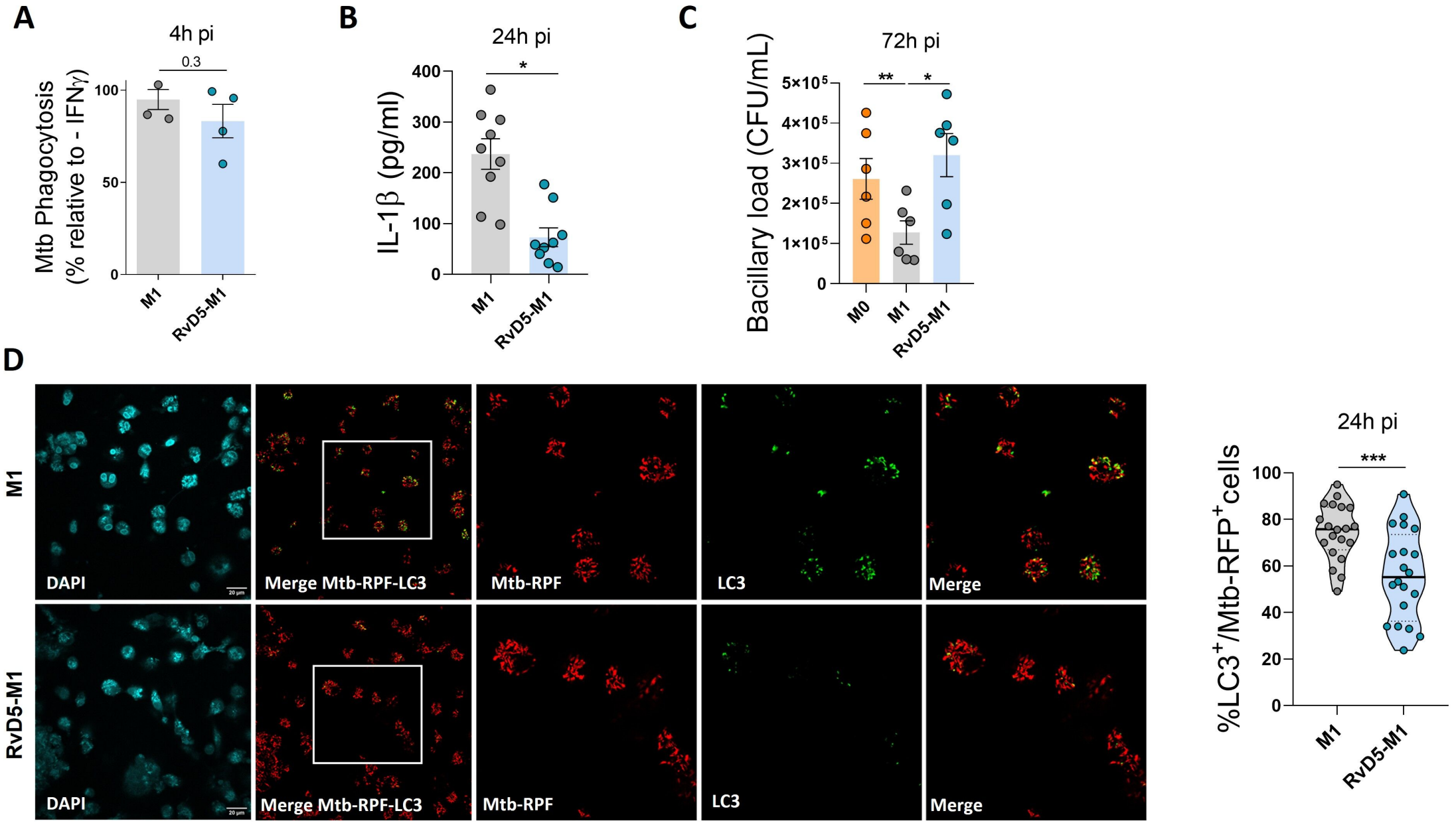
A
4h pi
0.3
Mtb Phagocytosis
(% relative to - IFNγ)
100
50
0
M1
RvD5-M1
B
24h pi
*
IL-1β (pg/ml)
400
300
200
100
0
M1
RvD5-M1
C
72h pi
**
*
Bacillary load (CFU/mL)
5×10⁵
4×10⁵
3×10⁵
2×10⁵
1×10⁵
0
M0
M1
RvD5-M1
D
M1
RvD5-M1
DAPI
Merge Mtb-RPF-LC3
Mtb-RPF
LC3
Merge
24h pi
***
%LC3⁺/Mtb-RFP⁺cells
100
80
60
40
20
0
M1
RvD5-M1

Figure 6

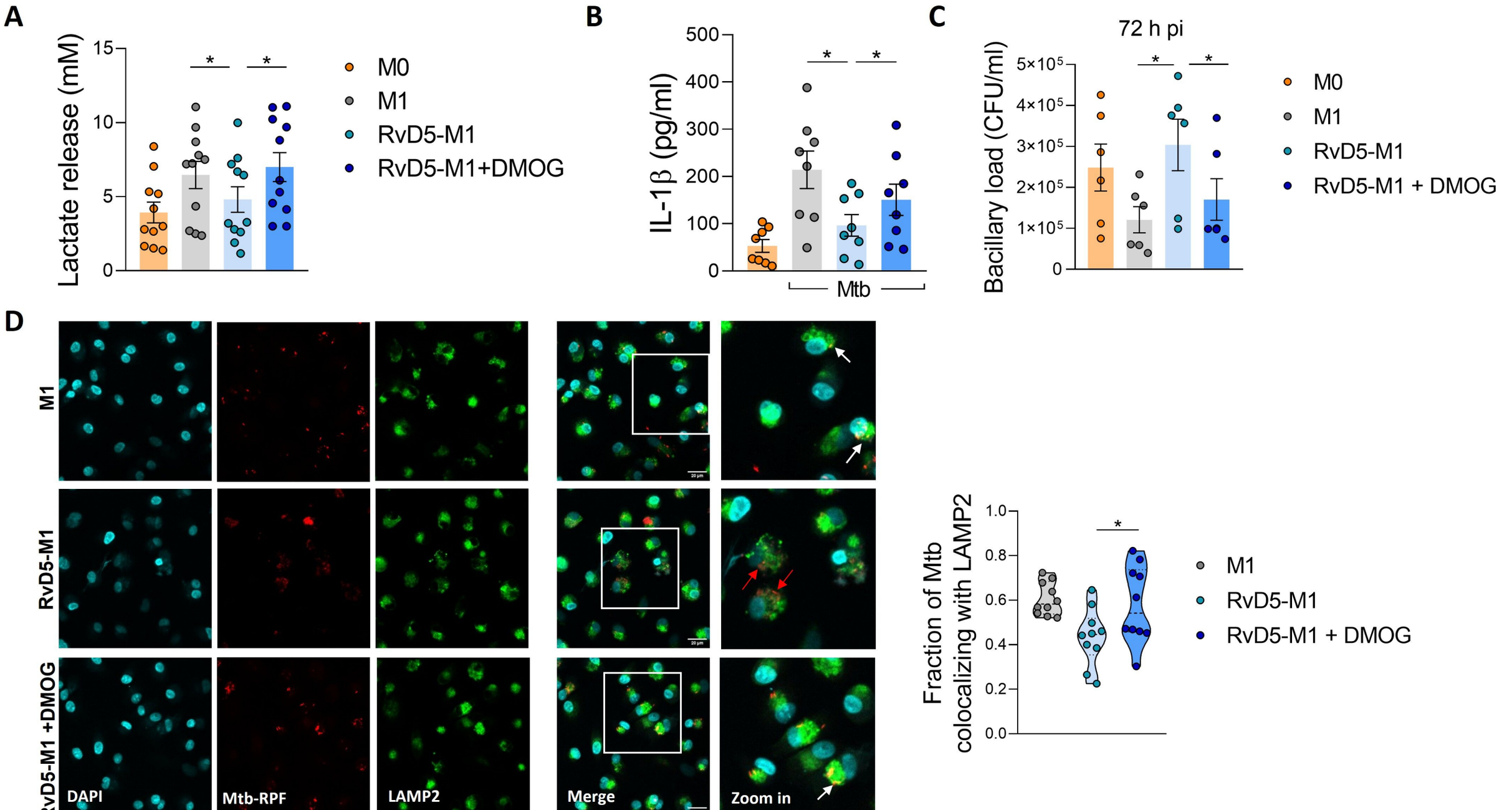
A
Lactate release (mM)
15
10
5
0
*
*
M0
M1
RvD5-M1
RvD5-M1+DMOG
B
IL-1β (pg/ml)
500
400
300
200
100
0
*
*
Mtb
C
72 h pi
Bacillary load (CFU/ml)
5×10⁵
4×10⁵
3×10⁵
2×10⁵
1×10⁵
0
*
*
M0
M1
RvD5-M1
RvD5-M1 + DMOG
D
M1
RvD5-M1
RvD5-M1 +DMOG
DAPI
Mtb-RPF
LAMP2
Merge
Zoom in
Fraction of Mtb colocalizing with LAMP2
1.0
0.8
0.6
0.4
0.2
0.0
*
M1
RvD5-M1
RvD5-M1 + DMOG